Postnatal Alveologenesis Depends on FOXF1 Signaling in c-KIT$^+$ Endothelial Progenitor Cells

Xiaomeng Ren[1,2], Vladimir Ustiyan[1,2], Minzhe Guo[2], Guolun Wang[1,2], Craig Bolte[1,2], Yufang Zhang[1,2], Yan Xu[2], Jeffrey A. Whitsett[2], Tanya V. Kalin[2] and Vladimir V. Kalinichenko[1,2,3]*

[1]Center for Lung Regenerative Medicine, [2]Division of Pulmonary Biology and [3]Division of Developmental Biology, Perinatal Institute, Cincinnati Children's Research Foundation, 3333 Burnet Ave., Cincinnati, OH 45229; USA

Online supplementary methods

The data, analytic methods, and study materials will be made available upon request from the corresponding author of this manuscript to other researchers for purposes of reproducing the results or replicating the procedure. All animal studies were reviewed and approved by the Institutional Animal Care and Use Committee at the Cincinnati Children's Hospital Medical Center, Cincinnati, Ohio, USA and NIH guidelines for laboratory animal care and safety were strictly followed. Human lung tissues and sections were provided by the LungMAP Human Tissue Core at the University of Rochester directed by Gloria Pryhuber. Tissue for LungMAP was obtained via the non-profit United Network for Organ Sharing, International Institute for Advancement of Medicine and National Disease Research Interchange. Consent for use of tissue was overseen by the University of Rochester Research Subjects Review Board (RSR B00056775) and the Cincinnati Children's Hospital Medical Center Institutional Review Board (#20180852).

Transgenic mice and neonatal hyperoxia. *Foxf1*$^{+/-}$ mouse line was described previously (1). *Kit*$^{w\text{-}sh}$ mice we purchased from Jackson Lab. *Foxf1*$^{fl/fl}$ mice (2) were bred with *Pdgfb-iCreER* mice (3) to generate *Pdgfb-iCreER Foxf1*$^{fl/fl}$ offspring. In *Pdgfb-iCreER Foxf1*$^{fl/fl}$ mice, tamoxifen causes *Foxf1* deletion in endothelial cells but not in other cell types (2, 4). Tamoxifen (3 mg, Sigma) was given i.p. at P0.5 and P2.5. Newborn pups with nursing mothers were placed in 85% oxygen or room air (controls) for 3 days (P1-P3), 7 days (P1-P7) or 3 weeks (P1-P21). Nursing mothers were rotated between hyperoxia and room air to avoid maternal oxygen toxicity. Oxygen concentrations were monitored with a Miniox II monitor (Catalyst Research, Owings Mills, MD). After hyperoxia exposure, mice were returned to room air. For labeling of perfused lung vasculature, Isolectin-B4 – FITC conjugate (Vector Lab) was injected i.v. two hours prior to the lung harvest. Lung function was determined by a computer-controlled small animal ventilator Flexivent as previously described (5, 6). Animal studies were approved by the Animal Care and Use Committee of Cincinnati Children's Research Foundation.

Flow cytometry and adoptive transfer of endothelial progenitor cells. Flow cytometry was performed after enzyme-digestion of lung tissue as described (7, 8). Apoptotic endothelial cells were detected by Annexin V apoptosis detection kit APC (eBioscience). 7-AAD (eBioscience) was used for labeling of necrotic cells. BrdU incorporation was measured as described previously (2). Anti-CD45 (clone 30-F11), anti-CD31 (PECAM-1) (clone 390), anti-CD326 (clone G8.8), anti-c-KIT (clone 2B8), anti-VEGFR3 (clone AFL4), anti-LYVE1 (clone ALY7), anti-TIE2 (clone TEK4), anti-EMCN (clone V.7C7), anti-NRP1 (clone 3DS304M) and anti-BrdU (clone BU20A) were purchased from eBioscience. Intracellular labeling protocol with cell fixation and permeabilization was described previously (6). Anti-FLK1(clone Avas12), anti-CD34 (clone MEC14.7), anti-CD140a (clone APA5), anti-CD140b (clone APB5) and anti-VE-Cadherin (clone BV13) were purchased from BioLegend. Anti-EphB4 (clone 395810) and anti-FOXF1 (AF4798) were purchased from R&D systems. Anti-SCF (ab64677) was obtained from ABCAM. Stained cells were separated using a five-laser FACSAria II (BD Biosciences). For adoptive transfer of endothelial progenitor cells, c-KIT$^+$ ECs (c-KIT$^+$ PECAM-1$^+$ CD45$^-$) and c-KIT$^-$ ECs (c-KIT$^-$ PECAM-1$^+$ CD45$^-$) were FACS-sorted from lung tissue of donor P3 mice expressing the *tdTomato* transgene inserted into *Rosa 26* locus (Jackson Lab.; C57Bl/6 background). Sorted cells were injected into the facial vein of recipient mice. 20,000 cells were used for adoptive transfer in *Foxf1*$^{+/-}$ and control littermates (C57Bl/6 background). 60,000 cells were used for adoptive transfer in hyperoxia-treated C57Bl/6 wild type mice.

Single Cell RNAseq analysis. Drop-seq RNA analyses of human postnatal day 1 (PND1) and mouse postnatal day 7 (PND7) were performed at Cincinnati Children's Hospital Medical Center. Data are available at LGEA (https://www.lungmap.net/breath-entity-page/?entityType=none&entityId=&entityLabel=&experimentTypes[]=LMXT0000000016. Expression matrices were processed using Drop-seq tools (http://mccarrolllab.com/download/922/, version 1.12). For pro-filtering, we required that cells express more than 500 genes (transcript count > 0), and less than 10% of transcript counts mapped to mitochondrial genes. Genes with transcripts detected in less than 2 cells were removed. Transcript counts in each cell were normalized by dividing by the total number of transcripts in each cell multiplied by the median number of transcripts per cell. Seurat (9) was used to detect highly variable genes and perform principle component analysis-based dimension reduction. Reduced dimensions were used for cell cluster identification using the Jaccard-Louvain clustering algorithm (10). Endothelial cell clusters were defined as *PECAM1*$^{+}$ (or *CDH5*$^{+}$) and *PTPRC (CD45)*$^{-}$ cells. Endothelial cells were further dissected into *KIT*$^{+}$ (transcript count > 0) and *KIT*$^{-}$ (transcript count = 0). A binomial test based method (10) was used to identify differentially expressed genes in *KIT*$^{+}$ vs. *KIT*$^{-}$ endothelial cells.

RNA preparation and quantitative real-time RT-PCR (qRT-PCR). RNA was prepared from mouse lung tissue or FACS-sorted endothelial progenitor cells using the RNeasy micro kit (Qiagen). qRT-PCR was performed using a StepOnePlus Real-Time PCR system (Applied Biosystems) using TaqMan primers (Suppl. Table E1) (11-13). Reactions were analyzed in triplicate and expression normalized to *β-actin* mRNA.

Immunohistochemistry and immunofluorescence. Paraffin or frozen sections were prepared from neonatal lung tissue and stained with hematoxylin and eosin (H&E) or used for immunohistochemical staining as described (14-16). The following antibodies were used for immunohistochemistry: PECAM-1 (553370, BD Biosciences and BBA7, R&D Systems), c-KIT (3074, Cell Signaling), FOXF1 (17), NKX2.1 (18), RFP (600-401-379, Rockland), αSMA (A5228, Sigma), LYVE1 (ab14917, Abcam) and Endomucin (ab106100, Abcam). Antibody complexes were detected by avidin-horseradish peroxidase complex and DAB substrate (Vector Laboratories, Burlingame, CA). Sections were counterstained with either nuclear fast red or DAPI (both from Vector Lab). Morphometrical measurements were performed using the Image-1/Metamorph Imaging System (Universal Imaging, West Chester, PA) as described previously (5). For co-localization experiments, secondary antibodies conjugated with Alexa Fluor 488 or Alexa Fluor 594 (Invitrogen) were used (19, 20). Fluorescent images were obtained using a Zeiss Axioplan2 microscope equipped with an AxioCam MRm digital camera and AxioVision 4.3 Software (Carl Zeiss Microimaging, Thornwood, NY).

Chip-seq. Cross-linked chromatin was sonicated using Covaris S220 to 200-300 bp fragments. ChIP with FOXF1 antibodies (17, 21) was performed using SX-8G IP-STAR robot (Diagenode). ChIP-Seq libraries were prepared using ChIPmentation procedure and sequenced using Illumina HiSeq 2500 in the Cincinnati Children’s Hospital Gene Sequencing Core. Data analysis was performed using the BioWardrobe platform (22).

Statistical analysis. One-way ANOVA and Student’s T-test were used to determine statistical significance. Right skewed measurements were log-transformed to meet normality assumptions prior to analysis. P values less than 0.05 were considered significant. Values for all measurements were expressed as mean ± standard deviation (SD).

Supplemental References

1. Sen P, Dharmadhikari AV, Majewski T, Mohammad MA, Kalin TV, Zabielska J, Ren X, Bray M, Brown HM, Welty S, Thevananther S, Langston C, Szafranski P, Justice MJ, Kalinichenko VV, Gambin A, Belmont J, Stankiewicz P. Comparative analyses of lung transcriptomes in patients with alveolar capillary dysplasia with misalignment of pulmonary veins and in foxf1 heterozygous knockout mice. *PloS one* 2014; 9: e94390.
2. Ren X, Ustiyan V, Pradhan A, Cai Y, Havrilak JA, Bolte CS, Shannon JM, Kalin TV, Kalinichenko VV. FOXF1 transcription factor is required for formation of embryonic vasculature by regulating VEGF signaling in endothelial cells. *Circulation research* 2014; 115: 709-720.
3. Claxton S, Kostourou V, Jadeja S, Chambon P, Hodivala-Dilke K, Fruttiger M. Efficient, inducible Cre-recombinase activation in vascular endothelium. *Genesis* 2008; 46: 74-80.
4. Cai Y, Bolte C, Le T, Goda C, Xu Y, Kalin TV, Kalinichenko VV. FOXF1 maintains endothelial barrier function and prevents edema after lung injury. *Sci Signal* 2016; 9: ra40.
5. Xia H, Ren X, Bolte CS, Ustiyan V, Zhang Y, Shah TA, Kalin TV, Whitsett JA, Kalinichenko VV. Foxm1 regulates resolution of hyperoxic lung injury in newborns. *American journal of respiratory cell and molecular biology* 2015; 52: 611-621.
6. Ren X, Shah TA, Ustiyan V, Zhang Y, Shinn J, Chen G, Whitsett JA, Kalin TV, Kalinichenko VV. FOXM1 promotes allergen-induced goblet cell metaplasia and pulmonary inflammation. *Molecular and cellular biology* 2013; 33: 371-386.
7. Ren X, Zhang Y, Snyder J, Cross ER, Shah TA, Kalin TV, Kalinichenko VV. Forkhead box M1 transcription factor is required for macrophage recruitment during liver repair. *Molecular and cellular biology* 2010; 30: 5381-5393.
8. Balli D, Ren X, Chou FS, Cross E, Zhang Y, Kalinichenko VV, Kalin TV. Foxm1 transcription factor is required for macrophage migration during lung inflammation and tumor formation. *Oncogene* 2012; 31: 3875-3888.
9. Satija R, Farrell JA, Gennert D, Schier AF, Regev A. Spatial reconstruction of single-cell gene expression data. *Nature biotechnology* 2015; 33: 495-502.
10. Shekhar K, Lapan SW, Whitney IE, Tran NM, Macosko EZ, Kowalczyk M, Adiconis X, Levin JZ, Nemesh J, Goldman M, McCarroll SA, Cepko CL, Regev A, Sanes JR. Comprehensive Classification of Retinal Bipolar Neurons by Single-Cell Transcriptomics. *Cell* 2016; 166: 1308-1323 e1330.
11. Wang IC, Meliton L, Ren X, Zhang Y, Balli D, Snyder J, Whitsett JA, Kalinichenko VV, Kalin TV. Deletion of Forkhead Box M1 transcription factor from respiratory epithelial cells inhibits pulmonary tumorigenesis. *PloS one* 2009; 4: e6609.
12. Wang IC, Snyder J, Zhang Y, Lander J, Nakafuku Y, Lin J, Chen G, Kalin TV, Whitsett JA, Kalinichenko VV. Foxm1 Mediates Cross Talk between Kras/Mitogen-Activated Protein Kinase and Canonical Wnt Pathways during Development of Respiratory Epithelium. *Molecular and cellular biology* 2012; 32: 3838-3850.
13. Wang IC, Ustiyan V, Zhang Y, Cai Y, Kalin TV, Kalinichenko VV. Foxm1 transcription factor is required for the initiation of lung tumorigenesis by oncogenic Kras(G12D.). *Oncogene* 2014; 33: 5391-5396.
14. Kim IM, Zhou Y, Ramakrishna S, Hughes DE, Solway J, Costa RH, Kalinichenko VV. Functional characterization of evolutionary conserved DNA regions in forkhead box f1 gene locus. *The Journal of biological chemistry* 2005; 280: 37908-37916.
15. Kalinichenko VV, Gusarova GA, Shin B, Costa R. The Forkhead Box F1 Transcription Factor is Expressed in Brain and Head Mesenchyme during Mouse Embryonic Development. *Gene Expression Patterns* 2003; 3: 153-158.
16. Wang X, Bhattacharyya D, Dennewitz MB, Zhou Y, Kalinichenko VV, Lepe R, Costa RH. Rapid Hepatocyte Nuclear Translocation of the Forkhead Box M1B (FoxM1B)

Transcription factor Causes a Transient Increase in Size of Regenerating Transgenic Hepatocytes. *Gene Expression* 2003; 11: 149-162.
17. Hoggatt AM, Kim JR, Ustiyan V, Ren X, Kalin TV, Kalinichenko VV, Herring BP. The transcription factor Foxf1 binds to serum response factor and myocardin to regulate gene transcription in visceral smooth muscle cells. *The Journal of biological chemistry* 2013; 288: 28477-28487.
18. Ustiyan V, Zhang Y, Perl AK, Whitsett JA, Kalin TV, Kalinichenko VV. beta-catenin and Kras/Foxm1 signaling pathway are critical to restrict Sox9 in basal cells during pulmonary branching morphogenesis. *Dev Dyn* 2016; 245: 590-604.
19. Wang IC, Zhang Y, Snyder J, Sutherland MJ, Burhans MS, Shannon JM, Park HJ, Whitsett JA, Kalinichenko VV. Increased expression of FoxM1 transcription factor in respiratory epithelium inhibits lung sacculation and causes Clara cell hyperplasia. *Developmental biology* 2010; 347: 301-314.
20. Ustiyan V, Wert SE, Ikegami M, Wang IC, Kalin TV, Whitsett JA, Kalinichenko VV. Foxm1 transcription factor is critical for proliferation and differentiation of Clara cells during development of conducting airways. *Developmental biology* 2012; 370: 198-212.
21. Bolte C, Ren X, Tomley T, Ustiyan V, Pradhan A, Hoggatt A, Kalin TV, Herring BP, Kalinichenko VV. Forkhead box F2 regulation of platelet-derived growth factor and myocardin/serum response factor signaling is essential for intestinal development. *The Journal of biological chemistry* 2015; 290: 7563-7575.
22. Bolte C, Flood HM, Ren X, Jagannathan S, Barski A, Kalin TV, Kalinichenko VV. FOXF1 transcription factor promotes lung regeneration after partial pneumonectomy. *Sci Rep* 2017; 7: 10690.

Supplemental Table E1. qRT-PCR TaqMan gene expression assays.

Gene	Cat.#
Foxf1	Mm00487497_m1
Kit	Mm00445212_m1
Cdh5	Mm00486938_m1
Pecam1	Mm01242584_m1
β-actin	Mm00607939_s1

Supplemental Table E2. Overlap in gene expression changes between human and mouse endothelial progenitor cells isolated from neonatal lungs.

Gene	Name	**Human** c-KIT$^+$/c-KIT$^-$	**Human** *P* value	**Mouse** c-KIT$^+$/c-KIT$^-$	**Mouse** *P* value
Transcription Factors/ Nuclear Proteins					
AHNAK	AHNAK nucleoprotein (desmoyokin)	1.45	2.5E-04	1.36	9.5E-08
ANKRD11	Ankyrin repeat domain 11	1.38	1.1E-03	1.26	1.3E-05
ANKRD12	Ankyrin repeat domain 12	1.39	1.6E-03	1.35	1.8E-04
ARID4B	AT-rich interaction domain 4B	1.39	4.2E-03	1.26	2.2E-04
CASZ1	Castor zinc finger 1	1.9	7.1E-04	1.43	4.9E-09
CHD6	Chromodomain helicase DNA binding protein 6	2.0	9.1E-05	1.70	1.7E-09
DDX24	DEAD-box helicase 24	1.60	2.7E-03	1.39	5.8E-06
DDX46	DEAD-box helicase 46	1.49	3.6E-03	1.34	6.2E-06
DDX6	DEAD-box helicase 6	1.76	1.8E-03	1.29	2.3E-06
DEK	DEK proto-oncogene	1.46	1.6E-03	1.27	1.4E-05
EID1	EP300 interacting inhibitor of differentiation 1	1.61	1.4E-03	1.41	1.9E-08
ERG	ERG, ETS transcription factor	1.75	3.7E-04	1.31	6.4E-09
EWSR1	EWS RNA binding protein 1	1.88	1.8E-05	1.26	1.4E-04
FENDRR	FOXF1 adjacent non-coding developmental regulatory RNA	1.51	1.1E-03	1.31	2.1E-09
FOXF1	FOXF1, Forkhead box F1	1.60	6.1E-03	1.37	3.7E-06
FUS	FUS RNA binding protein	1.75	5.4E-05	1.26	1.3E-08
GPBP1	GC-rich promoter binding protein 1	1.72	2.4E-03	1.72	4.8E-11
HDAC7	Histone deacetylase 7	1.85	2.7E-05	1.35	1.7E-06
HMGN1	High mobility group nucleosome binding domain 1	1.64	5.0E-03	1.40	7.9E-12
HNRNPA0	Heterogeneous nuclear ribonucleoprotein A0	1.62	2.3E-03	1.43	1.1E-06
HNRNPA1	Heterogeneous nuclear ribonucleoprotein A1	1.83	5.7E-04	1.24	1.7E-04
HNRNPF	Heterogeneous nuclear ribonucleoprotein F	1.78	2.3E-03	1.32	1.2E-09
HNRNPH3	Heterogeneous nuclear ribonucleoprotein H3	1.67	3.5E-04	1.34	1.9E-04
HNRNPL	Heterogeneous nuclear ribonucleoprotein L	1.68	5.0E-03	1.57	3.7E-11
KLF6	Kruppel like factor 6	1.48	1.1E-03	1.25	1.7E-04
NEMF	Nuclear export mediator factor	1.67	1.3E-03	1.39	3.4E-05
NFIA	Nuclear factor I A	1.62	4.9E-03	1.35	3.4E-06

PPIG	Peptidylprolyl isomerase G	1.51	5.0E-04	1.23	1.9E-05
QKI	QKI, KH domain containing RNA binding	1.45	4.6E-04	1.34	6.6E-08
S100A16	S100 calcium binding protein A16	1.93	4.3E-04	1.22	2.5E-11
SAFB2	Scaffold attachment factor B2	1.77	2.0E-03	1.46	3.2E-07
SNRK	SNF related kinase	1.74	3.2E-03	1.42	3.8E-08
SNRPD3	Small nuclear ribonucleoprotein D3 polypeptide	1.81	1.9E-03	1.33	4.5E-09
SNU13	Small nuclear ribonucleoprotein 13	1.92	1.1E-03	1.58	2.7E-10
SOX18	SOX18, SRY-box 18	1.83	2.6E-04	1.25	2.0E-03
SOX7	SOX7, SRY-box 7	1.64	5.0E-03	1.68	2.2E-10
TCIM	Transcriptional and immune response regulator	1.32	1.4E-04	1.67	1.5E-11
THRAP3	Thyroid hormone receptor associated protein 3	1.63	2.4E-03	1.25	1.3E-05
WWTR1	TAZ, WW domain containing transcription regulator 1	1.70	6.0E-05	1.80	9.6E-16
ZFP36L1	ZFP36 ring finger protein like 1	1.24	4.2E-03	1.30	8.8E-09
ZNF292	Zinc finger protein 292	1.68	2.8E-03	1.31	6.5E-04
ZNF503	Zinc finger protein 503	1.64	5.0E-03	1.62	2.7E-12
Receptors/ Adhesion Molecules					
ADGRL2	Adhesion G protein-coupled receptor L2	1.71	2.9E-06	1.39	2.0E-07
APLNR	Apelin receptor	1.59	3.1E-03	1.81	9.7E-19
BSG	Basigin (Ok blood group)	1.97	5.5E-04	1.21	1.7E-03
CAV1	Caveolin 1	1.21	2.2E-04	1.2	8.0E-14
CD34	CD34 molecule	1.33	1.9E-04	1.28	3.1E-08
CD36	CD36 molecule	1.84	2.4E-07	1.23	7.1E-12
CD93	CD93 molecule	1.56	1.1E-05	1.25	4.0E-14
CDH5	VE-cadherin (CD144)	1.30	1.9E-04	1.20	7.1E-07
EFNB1	Ephrin B1	1.65	3.7E-03	1.68	2.2E-10
EFNB2	Ephrin B2	1.68	5.0E-03	1.28	1.2E-05
EMCN	Endomucin	1.37	3.1E-05	1.49	1.9E-13
ENG	Endoglin (CD105)	1.61	1.9E-04	1.25	4.7E-05
IFNGR1	Interferon gamma receptor 1 (CD119)	1.56	1.0E-03	1.44	6.8E-09
JCAD	Junctional cadherin 5 associated	1.52	1.7E-04	1.37	6.1E-06
KDR	FLK1, VEGF Receptor 2 (CD309)	1.57	5.7E-06	1.21	4.2E-06
KIT	KIT proto-oncogene receptor tyrosine kinase (CD117)	558	2E-253	667	0.0E-00
ROBO4	Roundabout guidance receptor 4	1.70	5.6E-07	1.39	1.0E-04
TEK	TIE2 TEK receptor tyrosine kinase (CD202B)	1.82	5.0E-04	1.38	1.1E-10
THSD1	Thrombospondin type 1 domain containing 1	2.62	7.0E-10	1.96	9.3E-16
TSPAN12	Tetraspanin 12	1.37	2.4E-03	1.52	2.5E-06
TSPAN18	Tetraspanin 18	2.53	1.7E-07	1.25	1.4E-06
Secreted Proteins/ Extracellular Mediators					
AGRN	Agrin	1.49	1.7E-03	1.25	2.0E-03
EDN1	Endothelin 1	1.74	2.6E-07	1.29	6.9E-06
KITLG	KIT ligand (Stem cell factor)	1.69	3.6E-04	1.25	4.0E-07
SELENOP	Selenoprotein P	1.54	1.9E-03	1.21	5.3E-07
SH3BGRL	SH3 domain binding glutamate rich protein like	1.90	9.7E-04	1.22	8.0E-05
SPARCL1	SPARC like 1 (hevin)	1.40	7.5E-08	1.33	2.4E-14
TNFSF10	TNF superfamily member 10 (TRAIL)	1.40	1.0E-04	1.45	3.0E-11

Cytoplasmic Proteins/ Intracellular Mediators/ Enzymes/ Adaptor Proteins					
ABCF1	ATP binding cassette subfamily F member 1	1.89	4.6E-04	1.38	5.3E-08
ACTN4	Actinin alpha 4	1.43	2.2E-04	1.24	1.8E-08
ACTR2	ARP2 actin related protein 2 homolog	1.85	1.6E-04	1.30	3.4E-05
ADCY4	Adenylate cyclase 4	1.64	5.0E-03	1.23	2.9E-03
ALDH2	Aldehyde dehydrogenase 2 family member	1.84	2.5E-03	1.46	1.4E-10
APPL1	Adaptor protein, phosphotyrosine interacting with PH domain and leucine zipper 1	1.84	2.5E-03	1.6	7.4E-07
ARAP3	ArfGAP with RhoGAP domain, ankyrin repeat and PH domain 3	1.61	6.2E-04	1.50	1.3E-07
ARF1	ADP ribosylation factor 1	1.84	4.2E-04	1.21	4.5E-07
ARHGAP18	Rho GTPase activating protein 18	1.58	1.1E-04	1.70	7.4E-09
ARHGEF15	Rho guanine nucleotide exchange factor 15	1.68	2.8E-03	1.34	2.0E-04
ARPP19	cAMP regulated phosphoprotein 19	2.41	9.0E-06	1.33	3.9E-07
ATP5MPL	ATP synthase membrane subunit 6.8PL	1.70	3.7E-03	1.41	2.8E-11
CAPNS1	Calpain small subunit 1	1.86	7.5E-04	1.53	1.1E-08
CARHSP1	Calcium regulated heat stable protein 1	1.59	2.6E-03	1.42	7.6E-07
CCDC85B	Coiled-coil domain containing 85B	1.67	1.4E-05	1.39	1.5E-05
CLTC	Clathrin heavy chain	1.66	1.8E-03	1.25	6.0E-03
COPS9	COP9 signalosome subunit 9	1.86	2.1E-03	1.43	1.2E-07
DAZAP2	DAZ associated protein 2	1.66	2.4E-04	1.21	1.2E-02
DHRS7	Dehydrogenase/reductase 7	2.0	4.5E-04	1.56	6.1E-08
DLC1	DLC1 Rho GTPase activating protein	1.78	7.0E-04	1.73	8.1E-21
DOCK9	Dedicator of cytokinesis 9	1.68	2.8E-03	1.25	6.6E-03
DPYSL2	Dihydropyrimidinase like 2	1.52	5.8E-04	1.74	2.2E-16
DPYSL3	Dihydropyrimidinase like 3	1.91	4.4E-05	1.71	2.8E-08
DUSP6	Dual specificity phosphatase 6	1.84	3.0E-06	1.67	3.1E-22
EEF1D	Eukaryotic translation elongation factor 1 delta	1.48	1.0E-03	1.38	2.0E-05
EIF4H	Eukaryotic translation initiation factor 4H	1.78	3.1E-03	1.32	6.6E-05
EVA1B	eva-1 homolog B	1.71	2.6E-04	1.29	1.5E-03
FNBP1L	Formin binding protein 1 like	2.31	6.5E-05	1.36	9.4E-12
GBP4	Guanylate binding protein 4	1.72	5.2E-04	1.37	1.9E-05
GCC2	GRIP and coiled-coil domain containing 2	1.71	2.2E-04	1.42	1.5E-10
GIMAP4	GTPase, IMAP family member 4	1.82	1.1E-03	1.33	2.7E-09
GNB1	G protein subunit beta 1	1.57	1.8E-03	1.28	1.0E-04
GNB2	G protein subunit beta 2	1.56	6.1E-04	1.24	3.2E-04
GSTP1	Glutathione S-transferase pi 1	1.72	7.7E-06	1.26	5.8E-03
HPGD	15-hydroxyprostaglandin dehydrogenase	1.28	1.2E-04	1.20	1.2E-11
ITSN2	Intersectin 2	1.50	3.8E-03	1.38	2.6E-07
JUP	Junction plakoglobin	1.91	5.7E-07	1.50	8.1E-13
LARP7	La ribonucleoprotein domain family member 7	2.02	1.3E-05	1.55	1.7E-07
MAOA	Monoamine oxidase A	2.32	2.7E-05	1.44	3.8E-06
MAPK3	Mitogen-activated protein kinase 3 (ERK1)	1.72	2.4E-03	1.38	1.6E-05
MRFAP1	Morf4 family associated protein 1	1.90	3.8E-05	1.41	7.6E-11
MRPL20	Mitochondrial ribosomal protein L20	1.69	3.2E-03	1.35	6.9E-05
MYLK	Myosin light chain kinase	1.67	1.1E-03	1.23	3.1E-03
MYO1B	Myosin IB	1.77	1.3E-03	1.45	2.6E-05
MYO6	Myosin VI	1.50	1.3E-04	1.53	3.1E-07
NDUFA13	NADH:ubiquinone oxidoreductase subunit A13	1.59	3.6E-03	1.28	1.7E-05
NDUFB2	NADH:ubiquinone oxidoreductase subunit B2	1.69	3.2E-03	1.62	6.5E-10

NREP	Neuronal regeneration related protein	1.71	3.2E-03	1.27	5.5E-14
PALMD	Palmdelphin	1.78	1.5E-03	1.37	2.1E-07
PDIA6	Protein disulfide isomerase family A member 6	1.65	3.7E-03	1.35	4.3E-08
PEA15	Proliferation and apoptosis adaptor protein 15	1.57	1.6E-04	1.27	5.0E-05
PLK2	Polo like kinase 2	1.74	6.4E-05	1.25	1.9E-04
PRCP	Prolylcarboxypeptidase	1.68	2.4E-03	1.66	6.5E-17
PSMB6	Proteasome subunit beta 6	2.02	2.0E-04	1.24	2.8E-05
PTPN12	Protein tyrosine phosphatase, non-receptor type 12	1.94	6.7E-04	1.50	1.4E-06
RAB11B	RAB11B, member RAS oncogene family	1.85	4.8E-04	1.39	1.1E-05
RAB1A	RAB1A, member RAS oncogene family	1.69	3.2E-03	1.28	3.4E-07
RAB7A	RAB7A, member RAS oncogene family	1.74	2.1E-03	1.40	1.6E-07
RAC1	Rac family small GTPase 1	1.38	4.6E-03	1.65	1.3E-10
RALB	RAS like proto-oncogene B	2.11	1.1E-05	1.29	1.0E-05
RASIP1	Ras interacting protein 1	1.67	7.9E-05	1.47	2.7E-07
RDX	Radixin	1.40	1.6E-04	1.22	2.7E-09
RGCC	Regulator of cell cycle	1.50	1.4E-11	2.02	4.4E-38
RHOC	Ras homolog family member C	1.58	3.0E-03	1.33	8.1E-08
RPL18	Ribosomal protein L18	1.42	4.3E-04	1.21	8.0E-07
RPL28	Ribosomal protein L28	1.55	8.5E-05	1.24	1.6E-07
RPL29	Ribosomal protein L29	1.70	2.4E-03	1.24	4.6E-07
RPL36AL	Ribosomal protein L36a like	1.79	1.4E-04	1.28	2.0E-07
RPN2	Ribophorin II	1.87	2.7E-05	1.60	3.1E-09
RSRC2	Arginine and serine rich coiled-coil 2	1.72	6.2E-05	1.30	3.5E-08
SDCBP	Syndecan binding protein	1.64	3.2E-03	1.23	4.2E-05
SELENOF	Selenoprotein F	1.70	2.4E-03	1.26	1.1E-05
SGK1	Serum/glucocorticoid regulated kinase 1	1.40	3.0E-06	1.32	7.2E-11
SKAP2	Src kinase associated phosphoprotein 2	2.19	7.3E-05	1.47	7.4E-07
SKP1	S-phase kinase associated protein 1	1.59	3.6E-03	1.36	1.1E-10
TMBIM6	Transmembrane BAX inhibitor motif containing 6	1.41	2.0E-03	1.34	6.5E-09
TMEM258	Transmembrane protein 258	2.11	2.0E-04	1.45	4.9E-12
TOMM7	Translocase of outer mitochondrial membrane 7	1.55	1.4E-03	1.30	6.1E-08
TTC3	Tetratricopeptide repeat domain 3	1.48	4.0E-03	1.30	1.0E-03
VAT1	Vesicle amine transport 1	1.69	2.6E-04	1.50	4.4E-06
WDR1	WD repeat domain 1	1.65	4.3E-03	1.35	1.8E-04

Bioinformatic analysis of single cell RNAseq was performed separately between human c-KIT$^+$ ECs (n=92) and c-KIT$^-$ ECs (n=558) and mouse c-KIT$^+$ ECs (n=383) and c-KIT$^-$ ECs (n=667). Table shows statistically significant similarities in gene expression changes between human and mouse EC progenitors. Expression levels are presented as c-KIT$^+$EC/c-KIT$^-$EC ratios. FOXF1 target genes are shown in red.

Supplemental Table E3. FOXF1-binding DNA regions identified by ChIPseq of mouse fetal lung MFLM-91U cells.

				Binding sites		
GENE	**TXSTART**	**STRAND**	**CHROM**	**1**	**2**	**3**
Ahnak	8989284	+	chr19	326 / 574		
Carhsp1	8672153	-	chr16	-849 / -564		
Cav1	17306335	+	chr6	-682 / -196		
Ddx24	103425867	-	chr12	-151 / 454		
Ddx46	55635027	+	chr13	-19 / 124		
Dpysl3	43393331	-	chr18	301 / 739		
Dusp6	99263231	+	chr10	-488 / 145	-1070 / -847	
Edn1	42301270	+	chr13	177 / 473		
Eif4h	134639328	-	chr5	-1336 / -717		
Fendrr	121084386	-	chr8	-66 / -489		
Foxf1	121084386	+	chr8	237 / 402	-1287 / -864	
Gcc2	58255526	+	chr10	-653 / -301		
Hdac7	97831767	-	chr15	-330 / 710	-1252 / -961	
Hnrnpa1	103239816	-	chr15	-260 / -7	520 / 663	
Hnrnpf	117906782	+	chr6	-868 / -497	-905 / -757	
Jup	100397790	-	chr11	-74 / 516		
Larp7	127553489	+	chr3	636 / 904		
Mapk3	126759626	+	chr7	671 / 1363		
Mrfap1	36796754	-	chr5	474 / 962		
Myo1b	51915974	-	chr1	-1142 / -909		
Ndufb2	39592583	+	chr6	-1141 / -951	-712 / 56	614 / 834
Ppig	69723088	+	chr2	-711 / -568		
Psmb6	70525357	+	chr11	-588 / -414		
Rab11b	33760486	-	chr17	38 / 184		
Sdcbp	6365680	+	chr4	-1139 / -347	801 / 1247	
Tmbim6	99392947	+	chr15	-587 / 359		
Tomm7	23844145	-	chr5	-974 / -711		
Ttc3	94371015	-	chr16	599 / 1136		
Wwtr1	57575910	-	chr3	-305 / 90		

SUPPLEMENTAL FIGURE LEGENDS

Supplemental Figure. E1. c-KIT$^+$ endothelial progenitor cells are present in the developing mouse lung. Immunostaining shows that c-KIT$^+$ co-localizes with PECAM-1 (arrowheads) in subset of EC of pulmonary blood vessels (V) and lung parenchyma of wild-type E16.5 and P7 mice (A) and human neonatal lung (B). Magnification: panel A, x400 (inserts are x1000); panel B, x200 (inserts are x1000);

Supplemental Figure. E2. c-KIT$^+$ endothelial progenitor cells express CD34. FACS analysis of collagenase-digested P7 mouse lungs shows that c-KIT$^+$ ECs (c-KIT$^+$ PECAM-1$^+$ CD45$^-$) express CD34. c-KIT$^+$ ECs are negative for CD140b (PDGFRb), CD140a (PDGFRa), CD326 (EPCAM), NRP1, EphB4 and LYVE1. Cell viability was determined by 7-AAD.

Supplemental Figure. E3. Gene ontology (GO) biological processes enriched in human and mouse c-KIT$^+$ endothelial progenitor cells. ***(A)*** Histograms show significantly enriched biological processes in human c-KIT$^+$ ECs (n=92 cells) compared to c-KIT$^-$ ECs (n=558) isolated from human postnatal day 1 lung (PND1). ToppGene software suite was used for functional enrichment analysis. ***(B)*** Histograms show significantly enriched biological processes in mouse c-KIT$^+$ ECs (n=383 cells) compared to c-KIT$^-$ ECs (n=667) isolated from mouse postnatal day 7 lung (PND7). Single-cell RNAseq datasets were obtained from the Lung Gene Expression Analysis (LGEA) Web Portal (https://research.cchmc.org/pbge/lunggens/mainportal.html).

Supplemental Figure. E4. Gene expression profile in mouse c-KIT$^+$ endothelial progenitor cells. ***(A)*** Heatmap visualization of genes differentially expressed in mouse c-KIT$^+$ ECs. A binomial test-based method was used to compare the expression of genes between 383 c-KIT$^+$ and 667 c-KIT$^-$ ECs isolated from mouse P7 lungs. Mouse single-cell RNAseq dataset was obtained from the Lung Gene Expression Analysis (LGEA) Web Portal (https://research.cchmc.org/pbge/lunggens/mainportal.html). Gene expression profiles were clustered using hierarchical clustering with Pearson's correlation-based distance and complete linkage. Gene expression was Z-score normalized for visualization. GENE-E (https://software.broadinstitute.org/GENE-E/) was used to perform hierarchical clustering and heatmap visualization of gene expression. ***(B)*** Violin plots of the expression of *Foxf1, Kit, Tek, Cdh5, Vwf* and *Cd34* in mouse c-KIT$^+$ and c-KIT$^-$ ECs. Grey points indicate the gene expression in individual cells, measured in Unique Molecular Identifier (UMI). P value was calculated by binomial test based differentially expression analysis. P value < 0.05 and the fold change > or equal 1.2 were considered as significant.

Supplemental Figure. E5. FOXF1-binding regions in promoters of endothelial genes identified by ChIPseq. Schematic of FOXF1-binding regions in promoters of *Dusp6, Mapk3, Psmb6, Ahnak, Cav1, Jup* and *Sdcbp*. ChIPseq was performed using mouse fetal lung endothelial MFLM-91U cell line. H3K4me3 methylation marks are shown for the same promoter regions. Regions of significant FOXF1 binding to chromatin are shown by star. Transcriptional start sites and direction of translation are shown with arrows.

Supplemental Figure. E6. FOXF1 binds to bidirectional promoter of *Foxf1* and *Fendrr*. Schematic of FOXF1-binding regions in *Foxf1*/ *Fendrr* bidirectional promoter. ChIPseq was performed using mouse fetal lung endothelial MFLM-91U cell line. Regions of significant FOXF1 binding to chromatin that contain HeK4me1 and H3K4me3 methylation marks are show by black boxes. Transcriptional start sites and direction of translation are shown with arrows.

Supplemental Figure. E7. FACS analysis shows the presence of FOXF1 protein in lung endothelial cells. Cell suspension from collagenase-digested P7 mouse lungs was used for intracellular staining with FOXF1 Ab. FOXF1 protein is detected in lung ECs (PECAM-1^{+} CD45^{-}) but not in epithelial cells (EpCAM^{+} CD45^{-}). Isotype control Ab is shown with dotted line.

Supplemental Figure. E8. Neonatal hyperoxia causes alveolar simplification and disrupts lung function. ***(A)*** Schematic representation of hyperoxia (HO) treatment of wild type (WT) newborn mice. Control mice were exposed to room air (RA). ***(B)*** H&E staining shows alveolar simplification in lungs of HO-treated mice at P30. Percentages of airspace were calculated using 10 random lung fields and n=5 mice per group. Scale bar is 50μm. ***(C)*** FlexiVent was used to assess lung function in 7-9 mice in each group. Measurements were carried out at P60. $p<0.05$ is *, $p<0.01$ is **, $p<0.001$ is *** and $p<0.0001$ is ****.

Supplemental Figure. E9. Neonatal hyperoxia decreases the number of endothelial and epithelial cells in the lung. ***(A)*** FACS analysis of collagenase-digested P30 mouse lungs shows decreased numbers of endothelial (EC, PECAM-1^{+}CD45^{-}) and epithelial cells (EpC, EpCAM^{+}CD45^{-}) after hyperoxia (HO) compared to room air exposure (RA). ***(B)*** FACS data are presented as numbers of EC, EpC and hematopoietic cells (HC, CD45^{+}) in 10^6 total lung cells (n=5 mice in each group). $p<0.01$ is **.

Supplemental Figure. E10. Deletion of *Foxf1* reduces *c-KIT* in pulmonary endothelial cells. ***(A-B)*** FACS analysis of collagenase-digested P7 mouse lungs shows decreased expression of cell surface and intracellular c-KIT proteins in endothelial cells from tamoxifen-treated *PDGFb-Cre/Foxf1$^{-/-}$* mice. Cell surface and intracellular c-KIT was distinguished using Abs recognizing cell surface or intracellular regions of c-KIT receptor. Percentages of cells are presented in panel B (n=5 mice per group). ***(C)*** ChIPseq shows FOXF1-binding regions and histone methylation marks within the mouse *Kit* gene locus. Mouse fetal lung endothelial MFLM-91U cell line was used for ChIPseq. Regions of significant FOXF1 binding to chromatin are shown by black boxes. Transcriptional start sites and direction of translation are shown with an arrow. ***(D-E)*** FACS shows a significant decrease in c-KIT$^+$ ECs in lungs of tamoxifen-treated *PDGFb-Cre/Foxf1*$^{+/-}$ and *PDGFb-Cre/Foxf1*$^{-/-}$ mice at P7 (n=4-6 mice in each group). $p<0.05$ is *, $p<0.01$ is **.

Supplemental Figure. E11. Deletion of *Foxf1* increases cell surface expression of SCF in pulmonary endothelial cells. *(A-B)* FACS analysis of collagenase-digested mouse lungs shows increased expression of SCF in FOXF1-negative endothelial cells using dot plots and histograms. Tamoxifen-treated *PDGFb-Cre/Foxf1*$^{-/-}$ and control *Foxf1*$^{fl/fl}$ lungs were harvested at P7. ***(C)*** Deletion of *Foxf1* increases SCF. Percentages of ECs expressing FOXF1 or SCF were calculated using n=4-5 mice in each group. $p<0.01$ is **.

Supplemental Figure E12. *Foxf1* haploinsufficiency increases endothelial cell death in the neonatal lung. FACS analysis shows a significant increase in cell death (Annexin V$^+$ 7AAD$^+$) among endothelial cell population (PECAM-1$^+$CD45$^-$) in *Foxf1*$^{+/-}$ lungs. Lungs of *Foxf1*$^{+/-}$ and WT littermates were harvested at P7 (n=5 mice in each group). $p<0.01$ is **.

Supplemental Figure E13. Deletion of *Foxf1* from endothelial cells decreases PECAM-1 staining in the neonatal lung. Immunostaining for PECAM-1 and TTF1 (NKX2.1) shows decreased PECAM-1 staining in tamoxifen-treated *PDGFb-Cre/Foxf1*$^{-/-}$ lungs. DAPI was used to stain cell nuclei. Sections were prepared from P7 lungs. Abbreviations: RA, room air; HO, hyperoxia. Scale bar is 20μm.

Supplemental Figure E14. Deletion of *c-Kit* decreases percentages of endothelial and epithelial cells in the neonatal lung. *(A)* Immunostaining for c-KIT, PECAM-1 and NKX2.1

shows the absence of c-KIT-positive endothelial cells in *Kit*$^{w\text{-}sh}$ lungs. Sections were prepared from P7 lungs. Abbreviations: RA, room air; HO, hyperoxia. Scale bar is 20μm. ***(B)*** FACS analysis shows a significant decrease in endothelial (PECAM-1^{+}CD45^{-}EpCAM^{-}) and epithelial cells (EpCAM^{+}CD45^{-}PECAM-1^{-}) in lungs of *Kit*$^{w\text{-}sh}$ mice. Lungs were harvested at P7 (n=4-5 mice in each group). p<0.01 is **.

Supplemental Figure E15. Adoptive transfer of c-KIT^{+} ECs increases capillary density and protects *Foxf1*$^{+/-}$ lungs from alveolar simplification. Cells were FACS-sorted from P3 lungs of *Rosa/tdTomato* donor mice and injected i.v. into hyperoxia-treated *Foxf1*$^{+/-}$ recipient mice at P3. Lungs were harvested at P14. ***(A)*** H&E staining shows diminished alveolarization in *Foxf1*$^{+/-}$ lungs, which was improved after adoptive transfer of donor c-KIT^{+} ECs (top panels). Immunostaining for endomucin (green) and NKX2.1 (red) shows the loss of endomucin in alveolar septa of hyperoxia-treated *Foxf1*$^{+/-}$ mice (arrowheads). DAPI was used to stain cell nuclei. Endomucin staining was improved after adoptive transfer of donor c-KIT^{+} ECs. Magnification: top panels, x200; middle panels, x400, bottom panels, x1500. ***(B)*** Quantification of endomucin staining was performed using ImageJ software in 10 random images from 5 mouse lungs in each group, p<0.05 is *, p<0.01 is **.

Supplemental Figure E16. FACS-sorted c-KIT^{+} ECs do not integrate into endothelium of large pulmonary arteries, vein and lymphatic vessels. ***(A)*** FACS analysis shows the absence of *tdTomato*$^{+}$ cells among epithelial (EpCAM^{+} PECAM-1^{-} CD45^{-}) and stromal (EpCAM^{-} PECAM-1^{-} CD45^{-}) cell populations in *Foxf1*$^{+/-}$ recipient lungs seven days after adoptive transfer (n= 5 mice). ***(B)*** Cells were FACS-sorted from P3 lungs of *Rosa/ tdTomato* donor mice and injected i.v. into *Foxf1*$^{+/-}$ P3 recipient mice that were exposed to hyperoxia from P1 to P3. Lungs were harvested at P14 and used for immunostaining for PECAM1, αSMA and LYVE-1. Slides were counterstained with DAPI. *tdTomato*-positive cells were not found in endothelium of large pulmonary arteries, vein and lymphatic vessels. Abbreviations: A, artery; V, vein; Ly, lymphatic vessel; EpC, epithelial cells; StC, stromal cells. Magnification is x1000.

Supplemental Figure. E17. Histological assessment of lung and heart structure after 3-day neonatal hyperoxia. H&E staining shows that 3-day hyperoxia exposure (P1-P3) does not lead to right ventricular hypertrophy (A) or obvious remodeling of pulmonary arteries (B) but causes alveolar simplification(C). Donor ECs were injected i.v. after hyperoxia exposure. Lungs were harvested at P30. Peripheral pulmonary blood vessels are shown with green arrowheads and inserts. Abbreviations: A, artery; Br, bronchiole; RV, right ventricle; LV, left ventricle; V, blood vessel. Magnification: A panels, x150; B panels, x400; C panels, x200 (inserts are x800).

Supplemental Figure E18. Adoptive transfer of c-KIT$^+$ ECs increases capillary density and decreases alveolar simplification in hyperoxia-treated wild type mice. Cells were FACS-sorted from lungs of *Rosa/tdTomato* donor mice and injected i.v. into hyperoxia-treated WT recipient mice. WT mice were exposed to HO between P1 and P3. ***(A)*** H&E staining shows diminished alveolarization in hyperoxia-treated P14 lungs, which was improved after adoptive transfer of donor c-KIT$^+$ ECs. Immunostaining for Endomucin (green) and NKX2.1 (red) shows the loss of Endomucin staining in hyperoxia-treated P14 lungs (arrowheads). DAPI was used to stain cell nuclei. Endomucin staining was increased after adoptive transfer of donor c-KIT$^+$ ECs. Magnification: top panels, x200; middle panels, x400, bottom panels, x1500. ***(B)*** Quantification of endomucin staining was performed using ImageJ software in 10 random images from 5 mouse lungs in each group. ***(C)*** Quantification of isolectin B4 staining shows that adoptive transfer of donor c-KIT$^+$ ECs increases alveolar capillary density after hyperoxia. P18 mice were i.v. injected with isolectin B4 and lungs were harvested two hours later. Perfused lung vasculature was imaged using confocal microscopy. 10 random 3D images were used for quantification (n=3-5 mice in each group), $p<0.05$ is *, $p<0.01$ is **.

Supplemental Figure E19. Adoptive transfer of c-KIT^{+} ECs increases the complexity of alveolar capillary networks in hyperoxia-treated wild type mice. Cells were FACS-sorted from lungs of P3 donor mice and injected i.v. into WT P3 recipient mice that were exposed to HO between P1 and P3. Immunostaining and confocal imaging for endomucin and NKX2.1 was performed at P14 (left panels). Confocal imaging for isolectin B4 was performed at P18 (right panels). Mice were i.v. injected with isolectin B4 2hr prior to the lung harvest. Isolectin B4 (green) shows perfused alveolar capillary networks. Adoptive transfer of c-KIT^{+} ECs increases capillary density after hyperoxia. Scale bars are 50μm.

Supplemental Figure E20. Confocal imaging of donor-derived cells in hyperoxia-treated recipient lungs. c-KIT^{+} ECs were FACS-sorted from P3 lungs of *Rosa/tdTomato* donor mice and injected i.v. into wild type P3 recipient mice that were exposed to hyperoxia between P1 and P3. At P18, mice were i.v. injected with isolectin B4 (green) and harvested two hours later. Perfused lung vasculature was imaged using confocal microscopy. Lungs of mice exposed to room air without cell transfer were used as controls for red autofluorescence. *tdTomato*-labeled cells are present in alveolar capillaries stained by Isolectin B4. Abbreviations: al, alveoli. Magnification: top and middle panels, x160; bottom panels, x640.

Supplemental Figure E21. Identification of donor-derived endothelial cells in recipient lungs by FACS analysis. ***(A-B)*** FACS analysis shows the presence of donor-derived *tdTomato*$^{+}$ endothelial cells at different time-points after adoptive transfer. c-KIT^{+} ECs were FACS-sorted from P3 lungs of *Rosa/tdTomato* donor mice and transferred to WT P3 recipient mice. Recipient mice were exposed to hyperoxia between P1 and P3. Lung tissue was harvested at different time-points after adoptive transfer and used for FACS analysis. Percentages of *tdTomato*$^+$ ECs cells are shown in B as mean ± SD (n=3-5 mice per group for each time point). Abbreviations: EC, endothelial cells; EpC, epithelial cells. ***(C-D)*** FACS analysis shows increased cell proliferation in donor-derived *tdTomato*$^+$ ECs compared to recipient (*tdTomato*$^-$) ECs. Lungs were harvested at P18. Hoechst 33342 was used to identify ECs undergoing S, G_2 and M phases of cell cycle (n=3 mice), $p<0.05$ is *, $p<0.01$ is **.

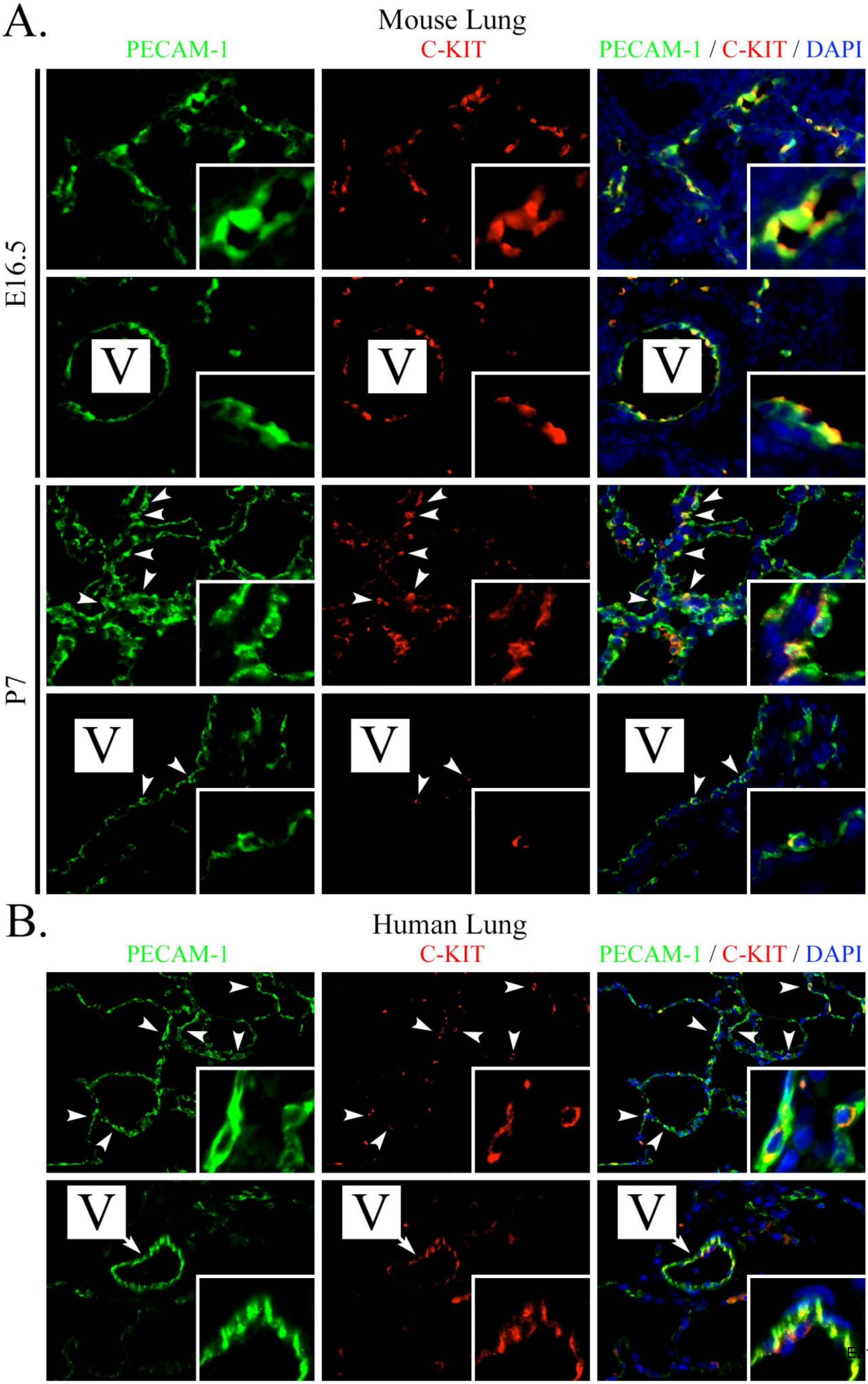
A.
Mouse Lung
PECAM-1
C-KIT
PECAM-1 / C-KIT / DAPI
E16.5
P7
V
B.
Human Lung
PECAM-1
C-KIT
PECAM-1 / C-KIT / DAPI
V

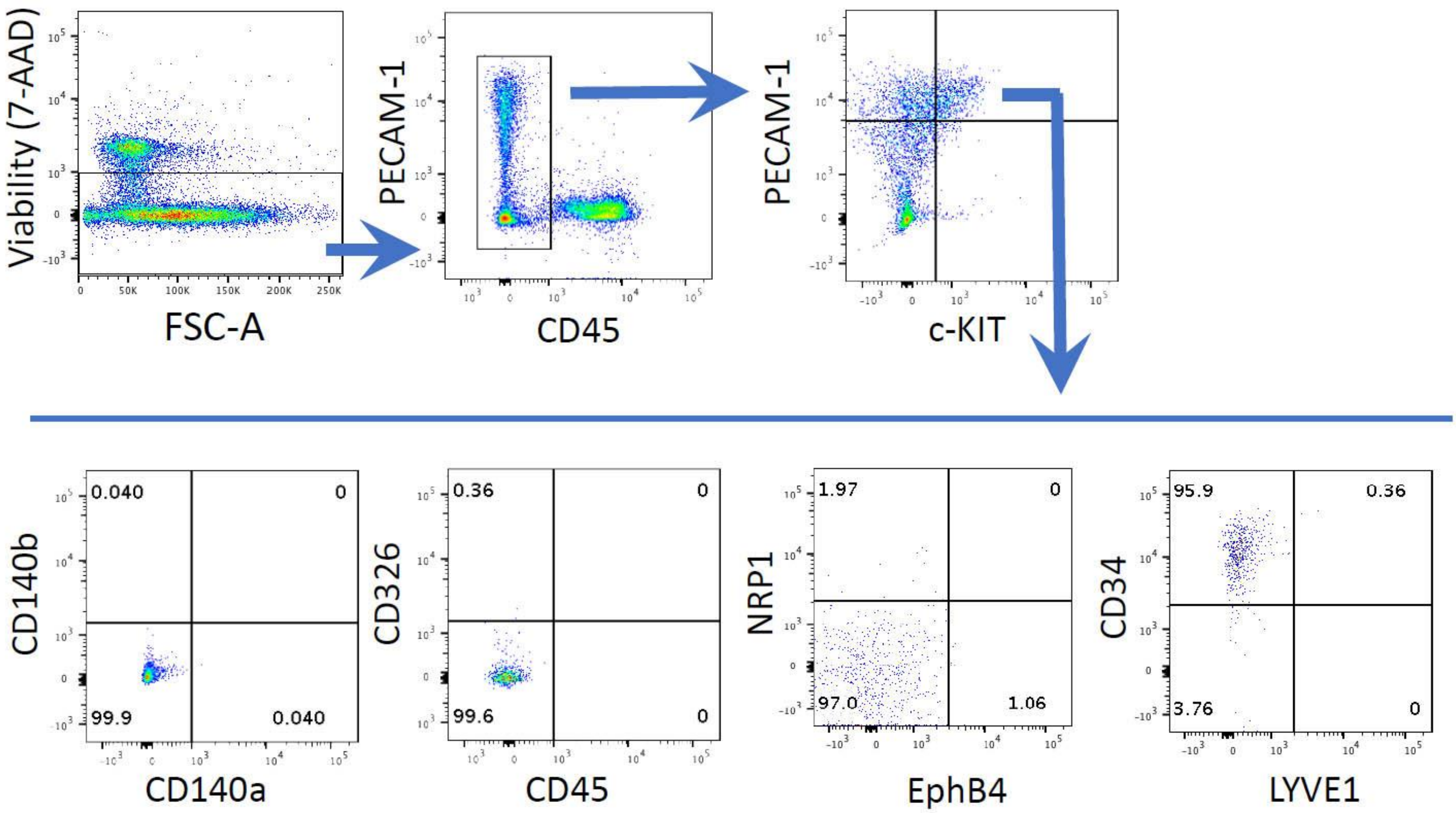
Viability (7-AAD)
FSC-A
PECAM-1
CD45
PECAM-1
c-KIT
CD140b
CD140a
0.040
0
99.9
0.040
CD326
CD45
0.36
0
99.6
0
NRP1
EphB4
1.97
0
97.0
1.06
CD34
LYVE1
95.9
0.36
3.76
0

A.

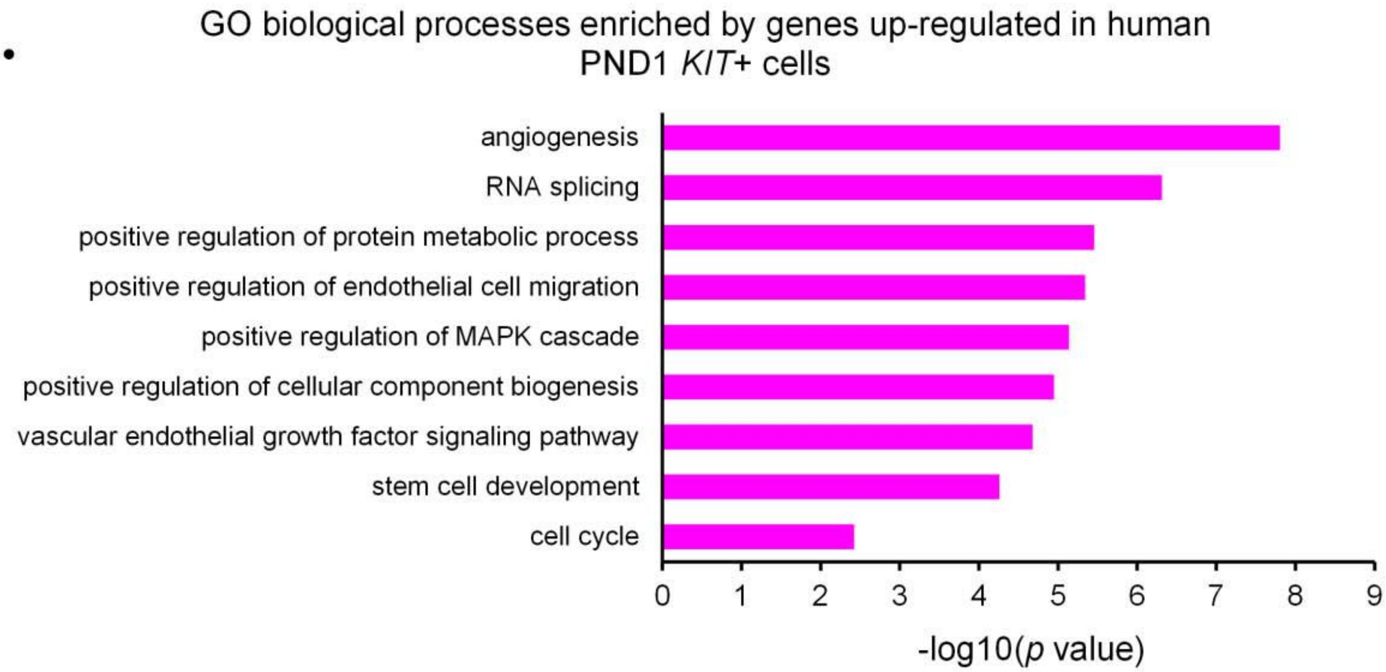
GO biological processes enriched by genes up-regulated in human
PND1 *KIT*+ cells
angiogenesis
RNA splicing
positive regulation of protein metabolic process
positive regulation of endothelial cell migration
positive regulation of MAPK cascade
positive regulation of cellular component biogenesis
vascular endothelial growth factor signaling pathway
stem cell development
cell cycle
0 1 2 3 4 5 6 7 8 9
-log10(*p* value)

B.

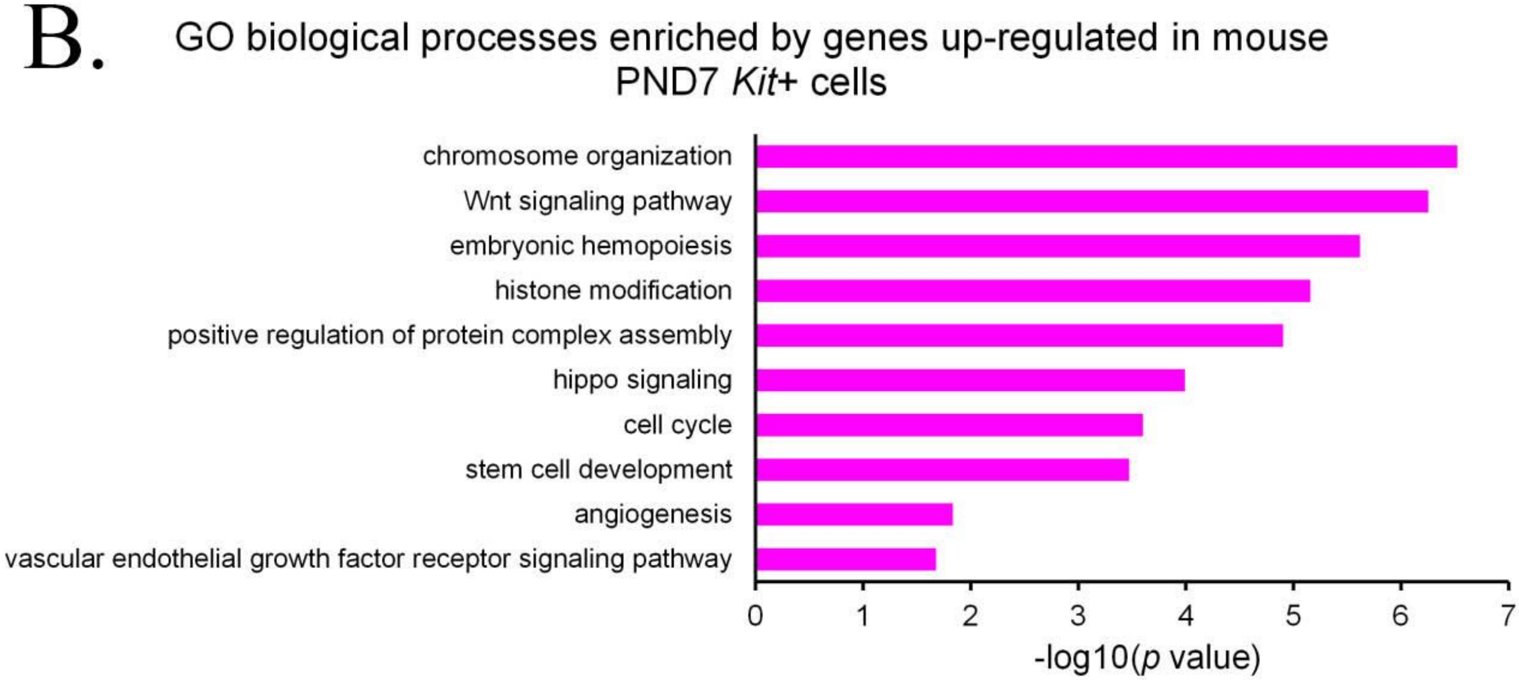
GO biological processes enriched by genes up-regulated in mouse
PND7 *Kit*+ cells
chromosome organization
Wnt signaling pathway
embryonic hemopoiesis
histone modification
positive regulation of protein complex assembly
hippo signaling
cell cycle
stem cell development
angiogenesis
vascular endothelial growth factor receptor signaling pathway
0 1 2 3 4 5 6 7
-log10(*p* value)

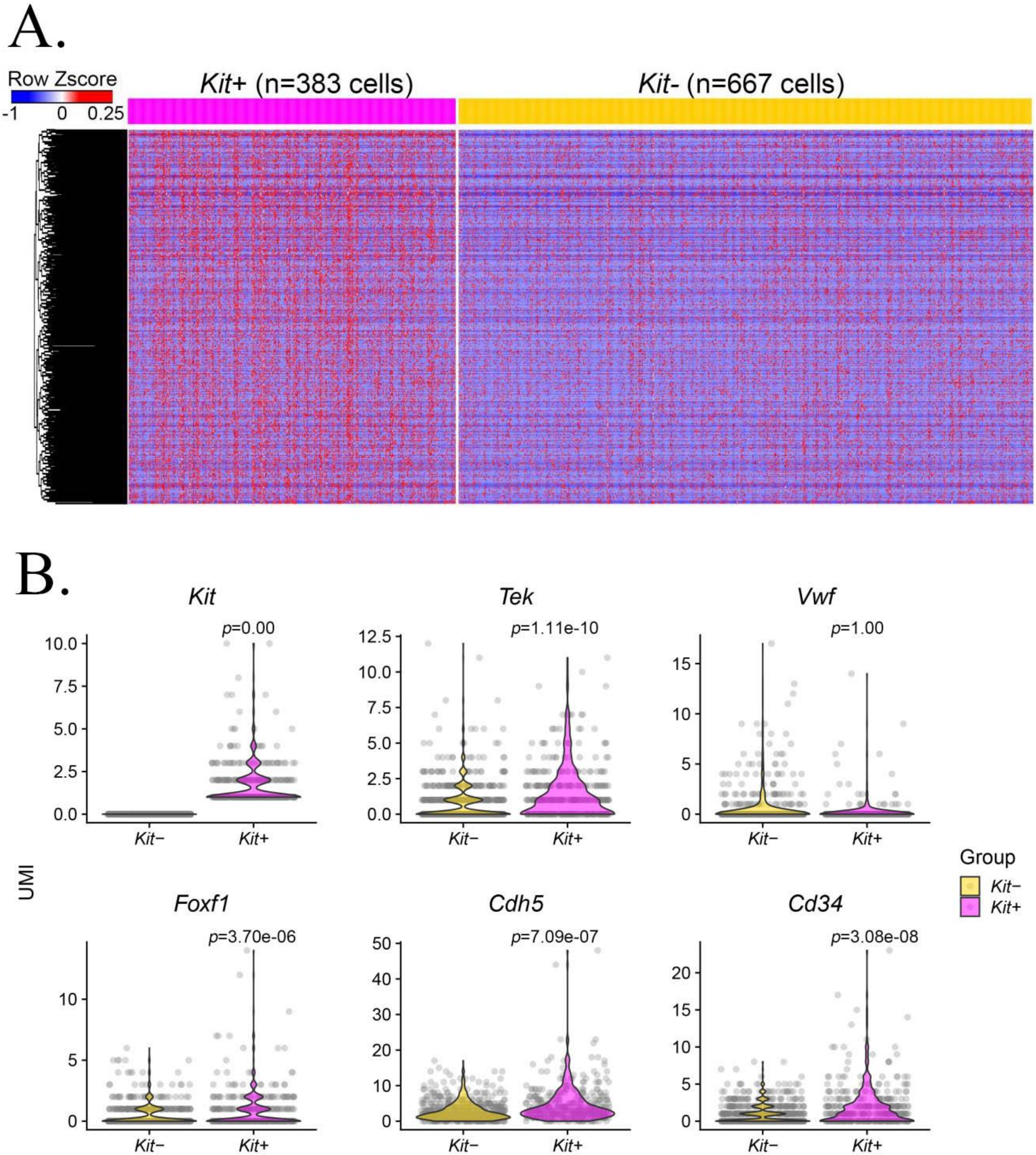
A.
Row Zscore
-1 0 0.25
Kit+ (n=383 cells)
Kit- (n=667 cells)
B.
Kit
p=0.00
Tek
p=1.11e-10
Vwf
p=1.00
Foxf1
p=3.70e-06
Cdh5
p=7.09e-07
Cd34
p=3.08e-08
UMI
Kit−
Kit+
Group
Kit−
Kit+

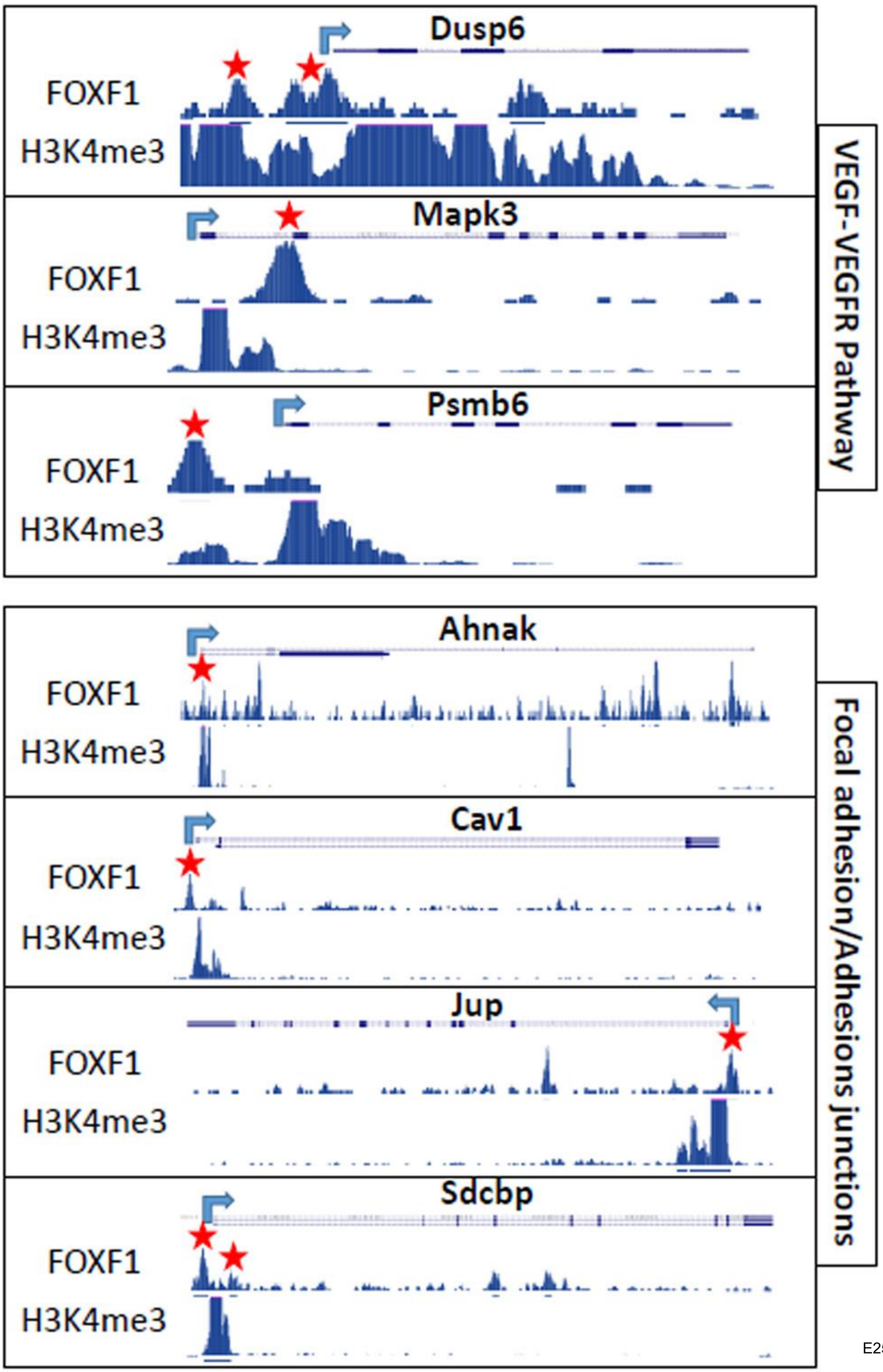
Dusp6
FOXF1
H3K4me3
Mapk3
FOXF1
H3K4me3
Psmb6
FOXF1
H3K4me3
VEGF-VEGFR Pathway
Ahnak
FOXF1
H3K4me3
Cav1
FOXF1
H3K4me3
Jup
FOXF1
H3K4me3
Sdcbp
FOXF1
H3K4me3
Focal adhesion/Adhesions junctions

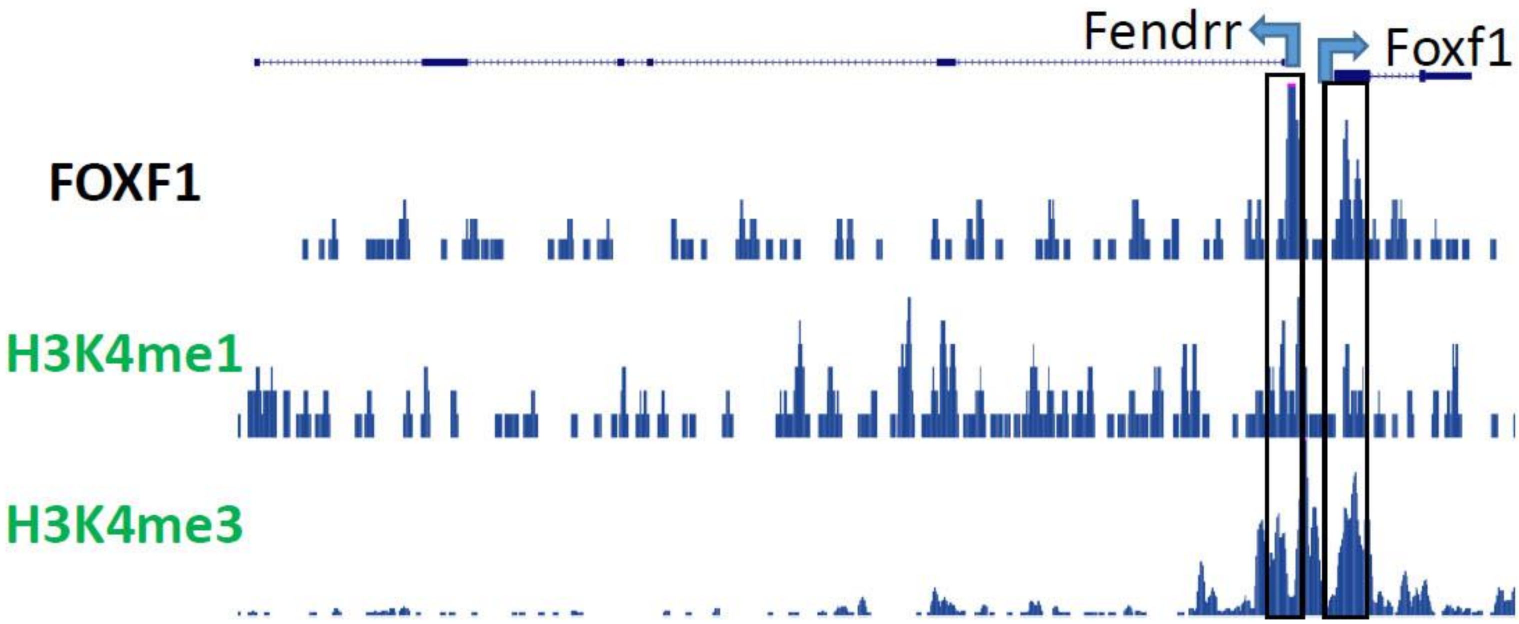
Fendrr
Foxf1
FOXF1
H3K4me1
H3K4me3

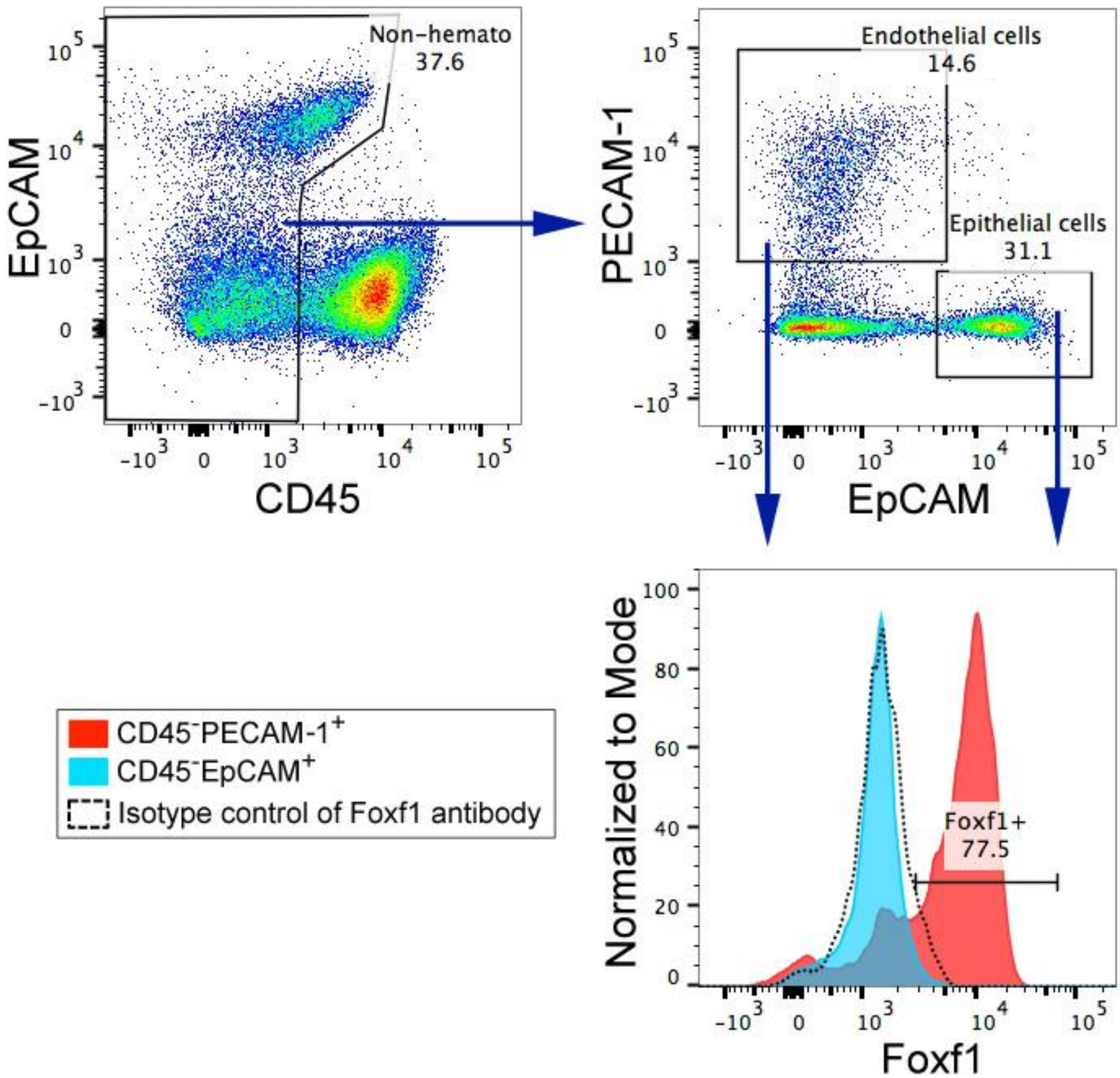

Non-hemato
37.6
EpCAM
CD45
Endothelial cells
14.6
Epithelial cells
31.1
PECAM-1
EpCAM
CD45⁻PECAM-1⁺
CD45⁻EpCAM⁺
Isotype control of Foxf1 antibody
Normalized to Mode
Foxf1+
77.5
Foxf1

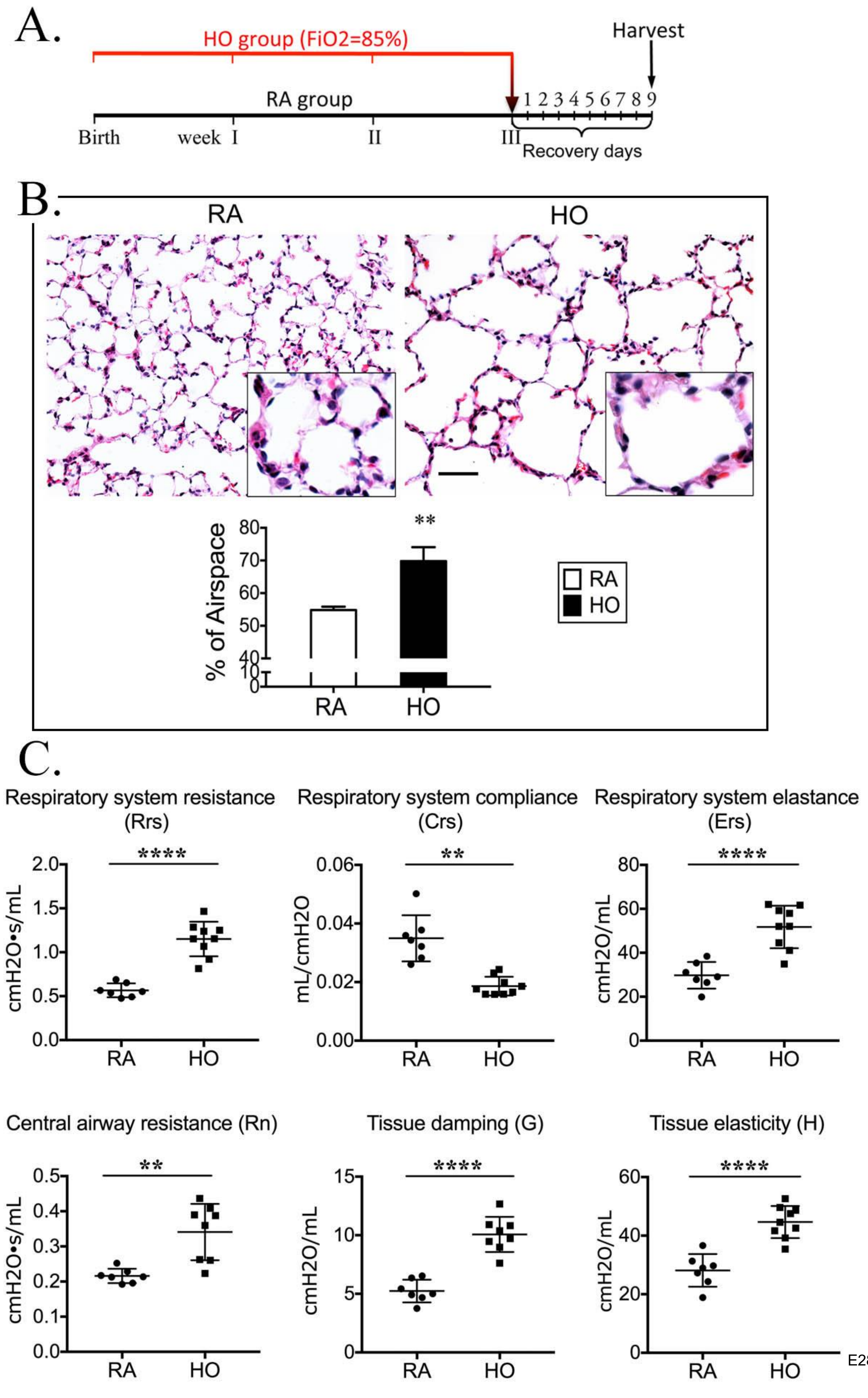
A.
HO group (FiO2=85%)
Harvest
RA group
1 2 3 4 5 6 7 8 9
Birth
week I
II
III
Recovery days
B.
RA
HO
% of Airspace
80
70
60
50
40
10
0
**
RA
HO
C.
Respiratory system resistance (Rrs)
cmH2O•s/mL
****
Respiratory system compliance (Crs)
mL/cmH2O
**
Respiratory system elastance (Ers)
cmH2O/mL
****
Central airway resistance (Rn)
cmH2O•s/mL
**
Tissue damping (G)
cmH2O/mL
****
Tissue elasticity (H)
cmH2O/mL
****

A.

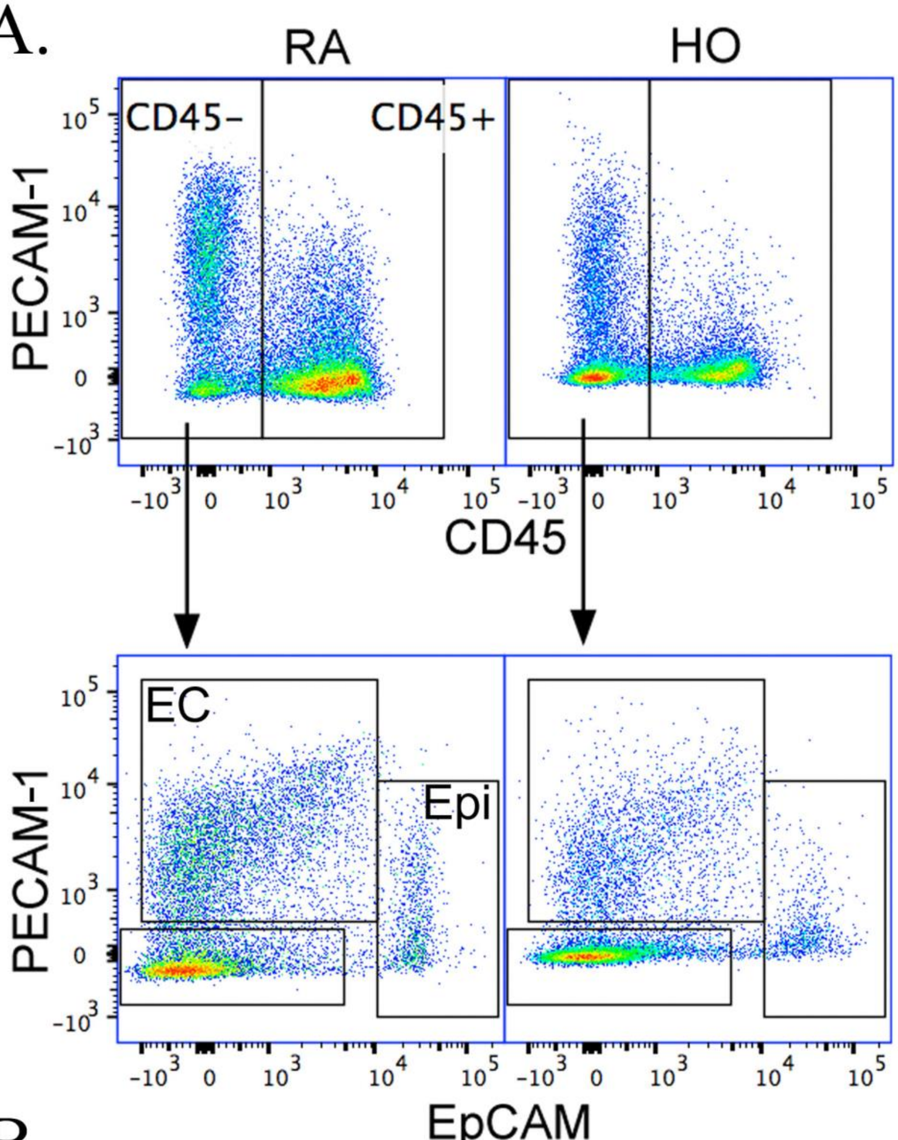
RA
HO
CD45−
CD45+
PECAM-1
CD45
EC
Epi
PECAM-1
EpCAM

B.

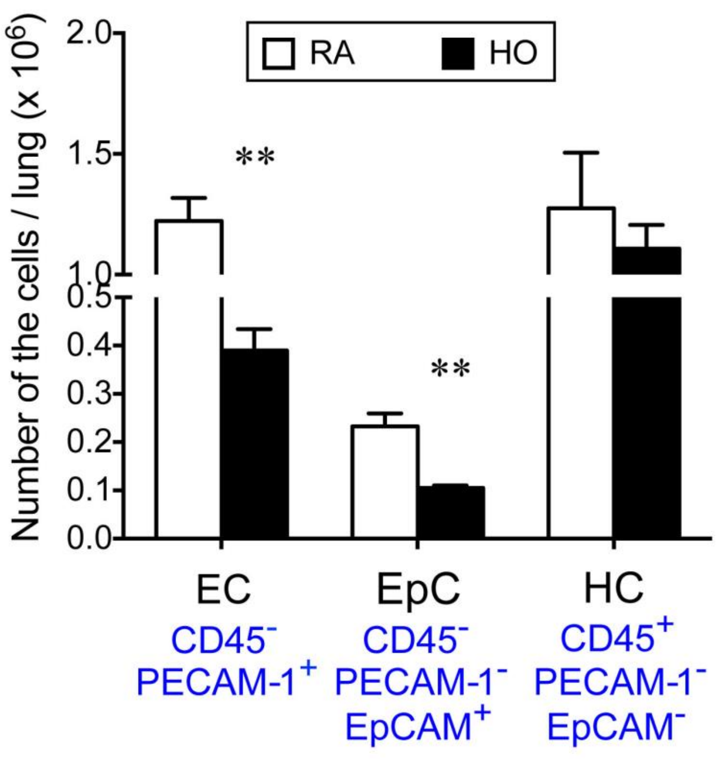
Number of the cells / lung (x 10^6)
RA
HO
**
**
EC
EpC
HC
CD45⁻ PECAM-1⁺
CD45⁻ PECAM-1⁻ EpCAM⁺
CD45⁺ PECAM-1⁻ EpCAM⁻

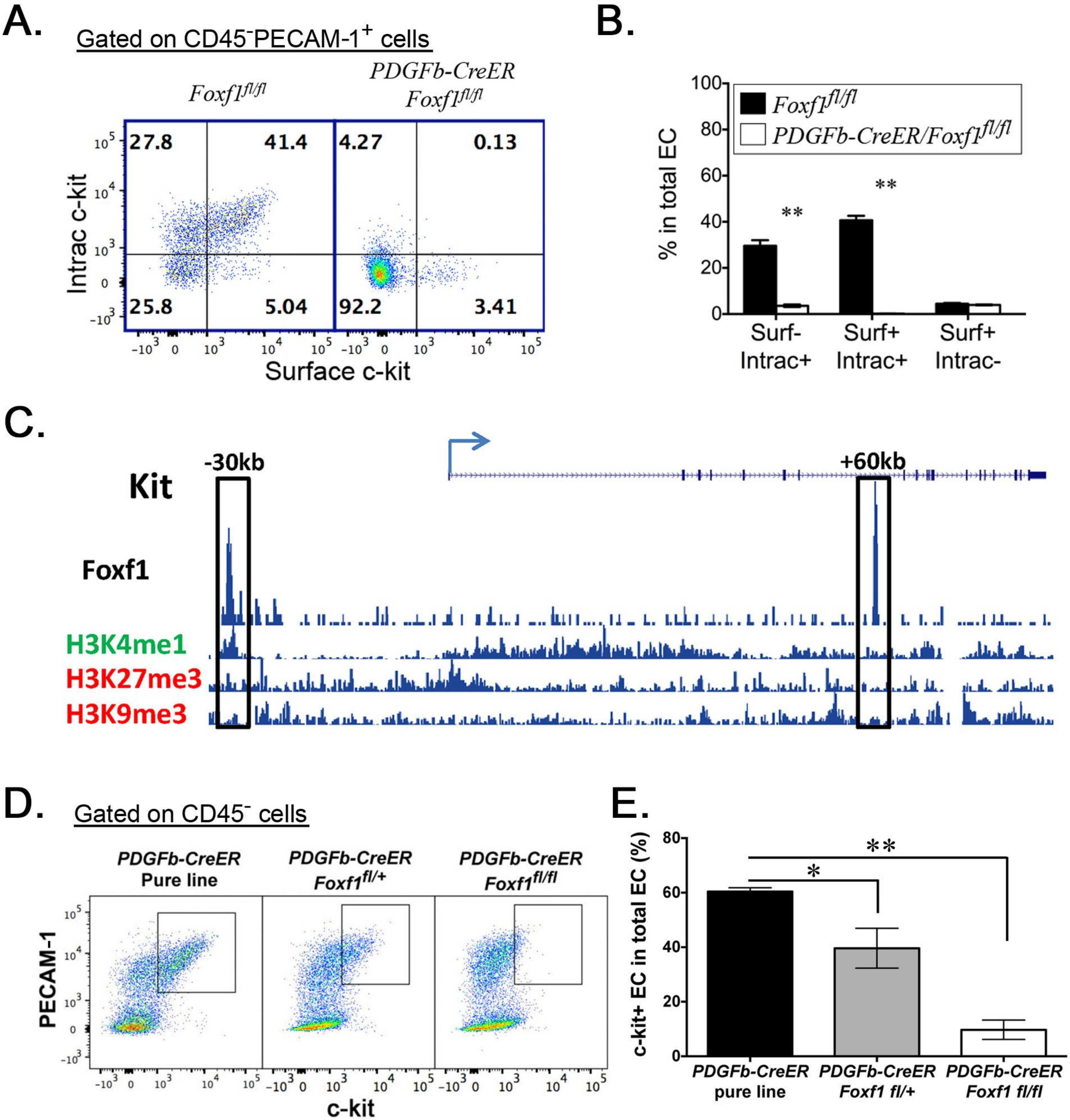
A.
Gated on CD45⁻PECAM-1⁺ cells
Foxf1fl/fl
PDGFb-CreER Foxf1fl/fl
27.8
41.4
25.8
5.04
4.27
0.13
92.2
3.41
Intrac c-kit
Surface c-kit
B.
Foxf1fl/fl
PDGFb-CreER/Foxf1fl/fl
% in total EC
**
**
Surf- Intrac+
Surf+ Intrac+
Surf+ Intrac-
C.
-30kb
+60kb
Kit
Foxf1
H3K4me1
H3K27me3
H3K9me3
D.
Gated on CD45⁻ cells
PDGFb-CreER Pure line
PDGFb-CreER Foxf1fl/+
PDGFb-CreER Foxf1fl/fl
PECAM-1
c-kit
E.
c-kit+ EC in total EC (%)
*
**
PDGFb-CreER pure line
PDGFb-CreER Foxf1 fl/+
PDGFb-CreER Foxf1 fl/fl

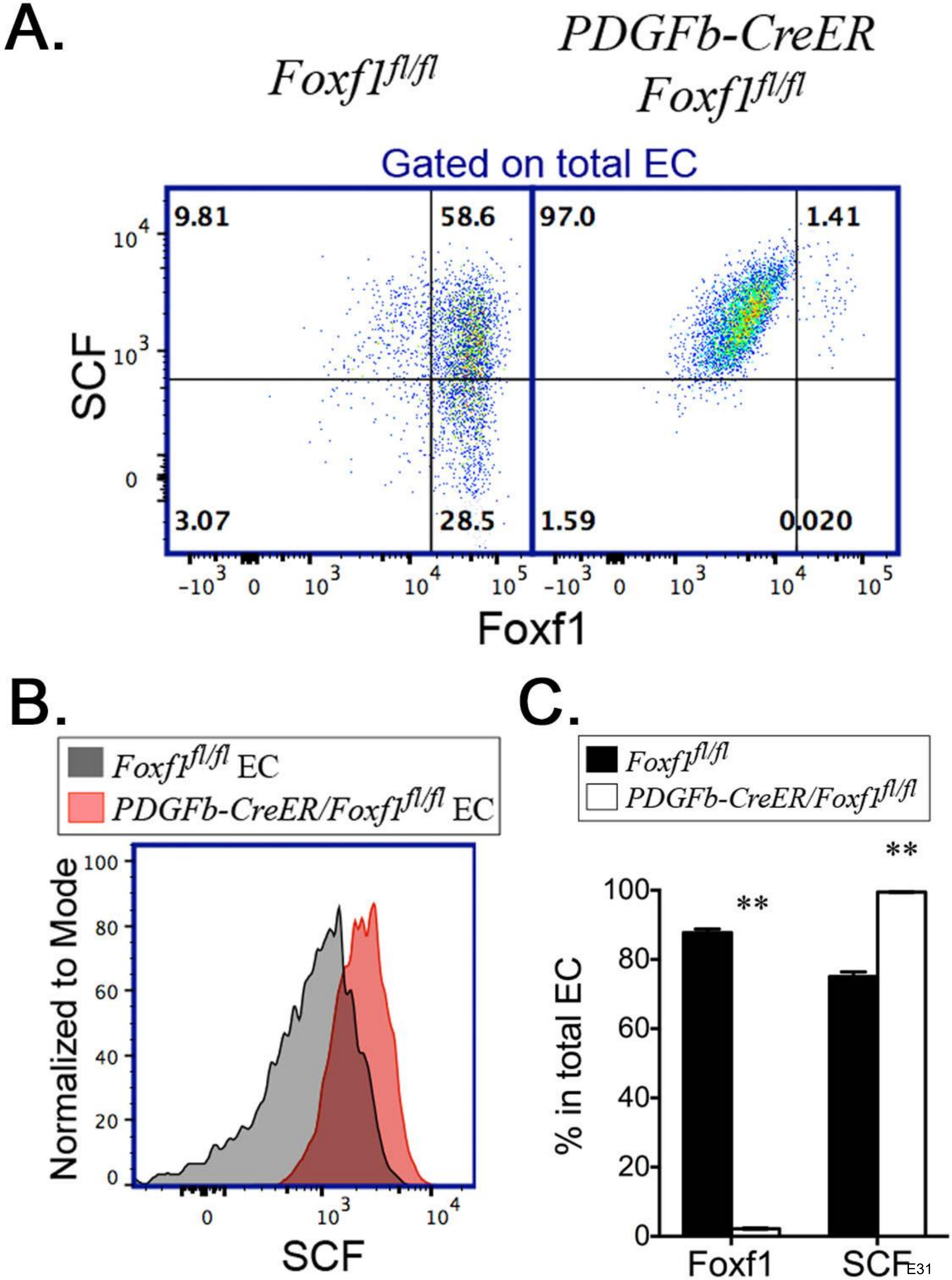
A.
Foxf1fl/fl
PDGFb-CreER
Foxf1fl/fl
Gated on total EC
9.81
58.6
3.07
28.5
97.0
1.41
1.59
0.020
SCF
Foxf1
B.
Foxf1fl/fl EC
PDGFb-CreER/Foxf1fl/fl EC
Normalized to Mode
SCF
C.
Foxf1fl/fl
PDGFb-CreER/Foxf1fl/fl
**
**
% in total EC
Foxf1
SCF

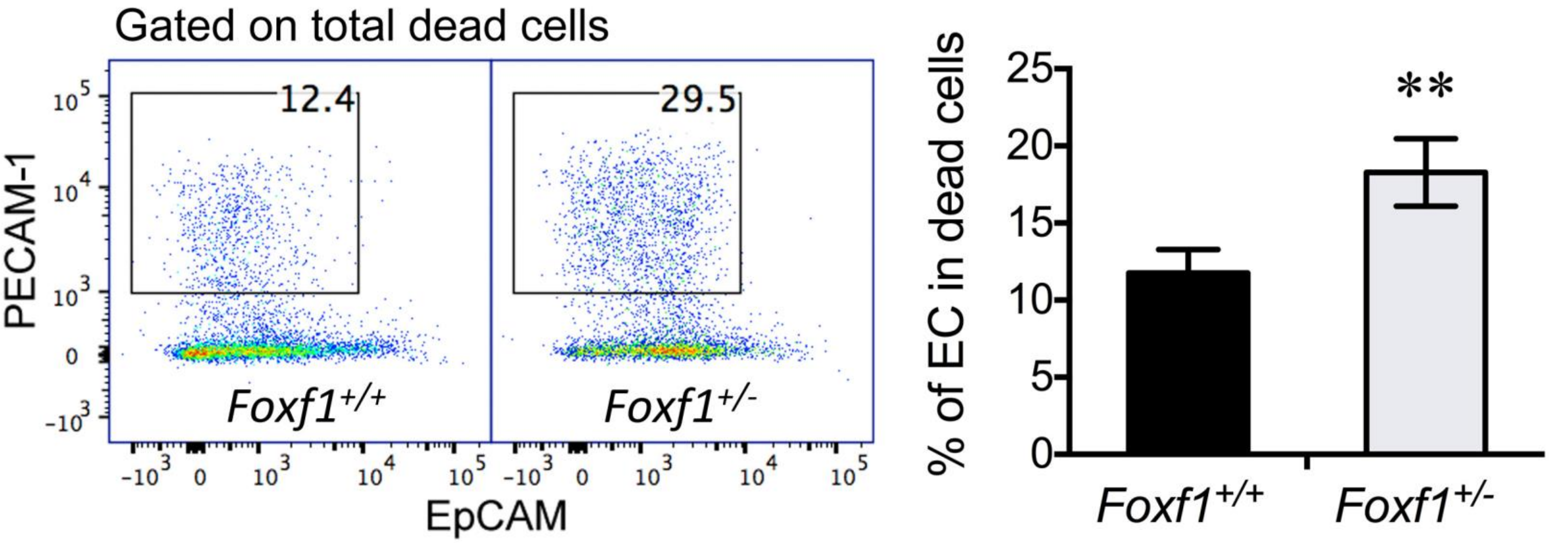
Gated on total dead cells
12.4
29.5
PECAM-1
Foxf1+/+
Foxf1+/-
EpCAM
% of EC in dead cells
**
Foxf1+/+
Foxf1+/-

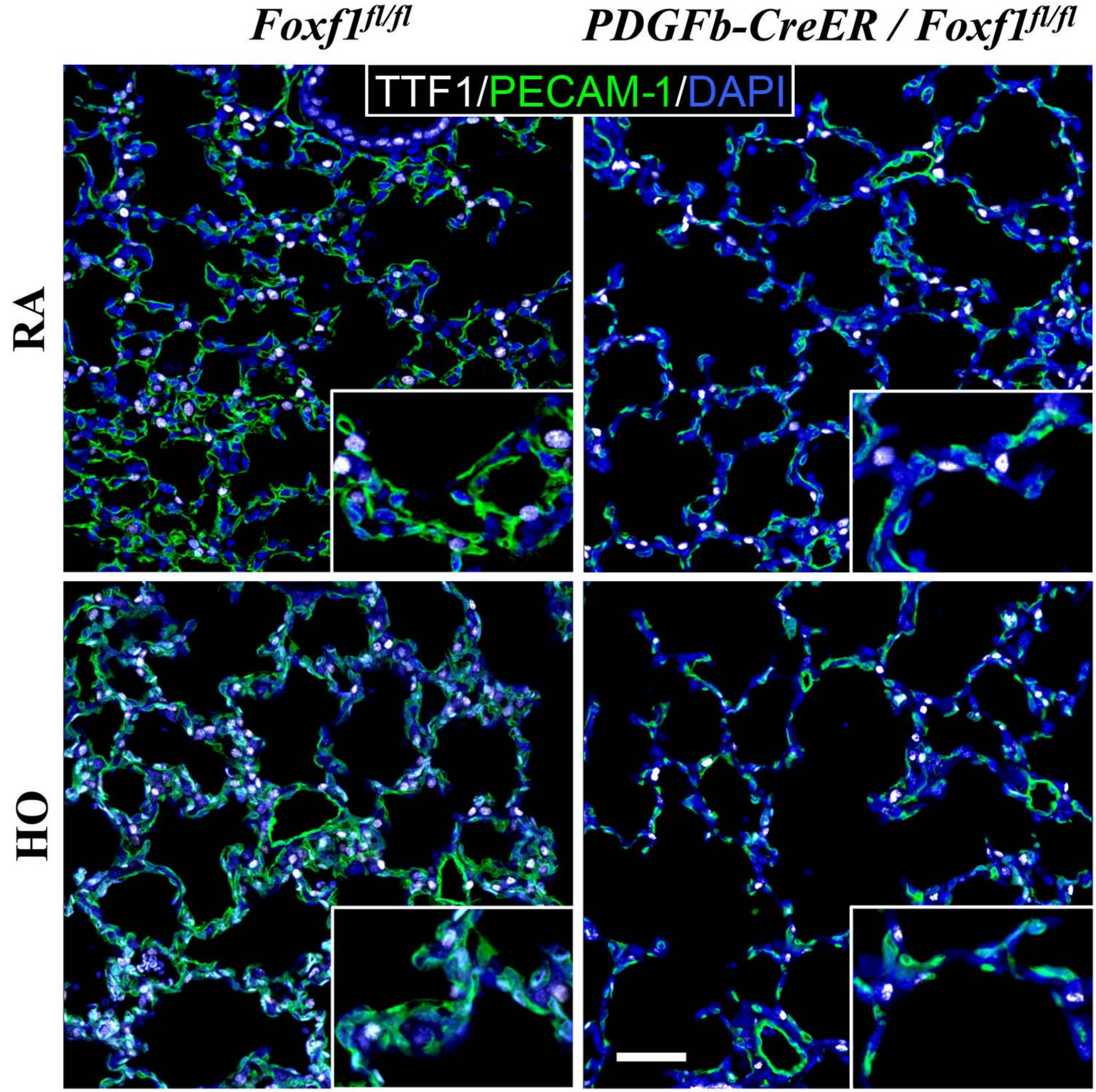
Foxf1fl/fl
PDGFb-CreER / Foxf1fl/fl
TTF1/PECAM-1/DAPI
RA
HO

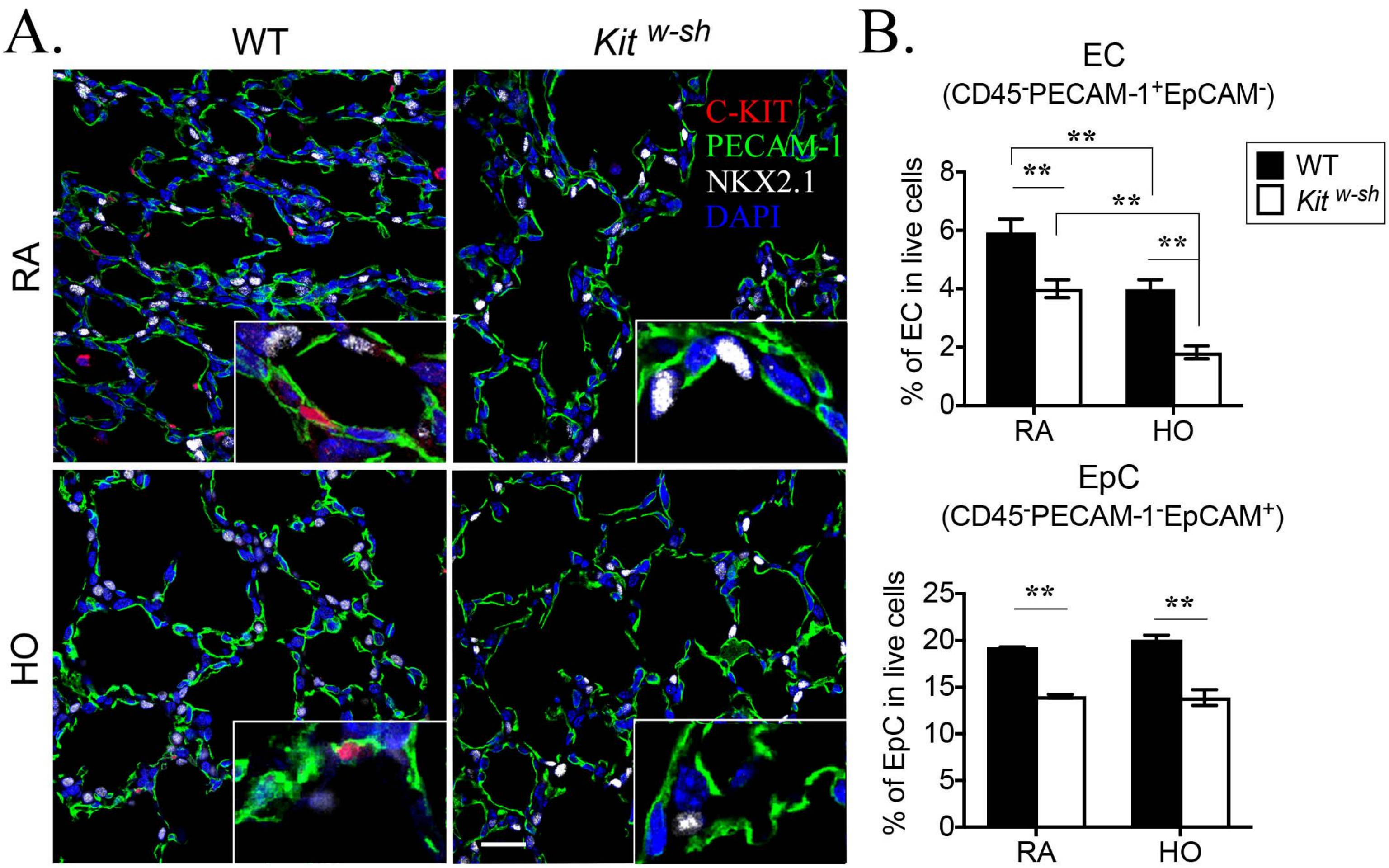
A.
WT
Kit w-sh
RA
HO
C-KIT
PECAM-1
NKX2.1
DAPI
B.
EC
(CD45-PECAM-1+EpCAM-)
% of EC in live cells
8
6
4
2
0
**
**
**
**
WT
Kit w-sh
RA
HO
EpC
(CD45-PECAM-1-EpCAM+)
% of EpC in live cells
25
20
15
10
5
0
**
**
RA
HO

A.

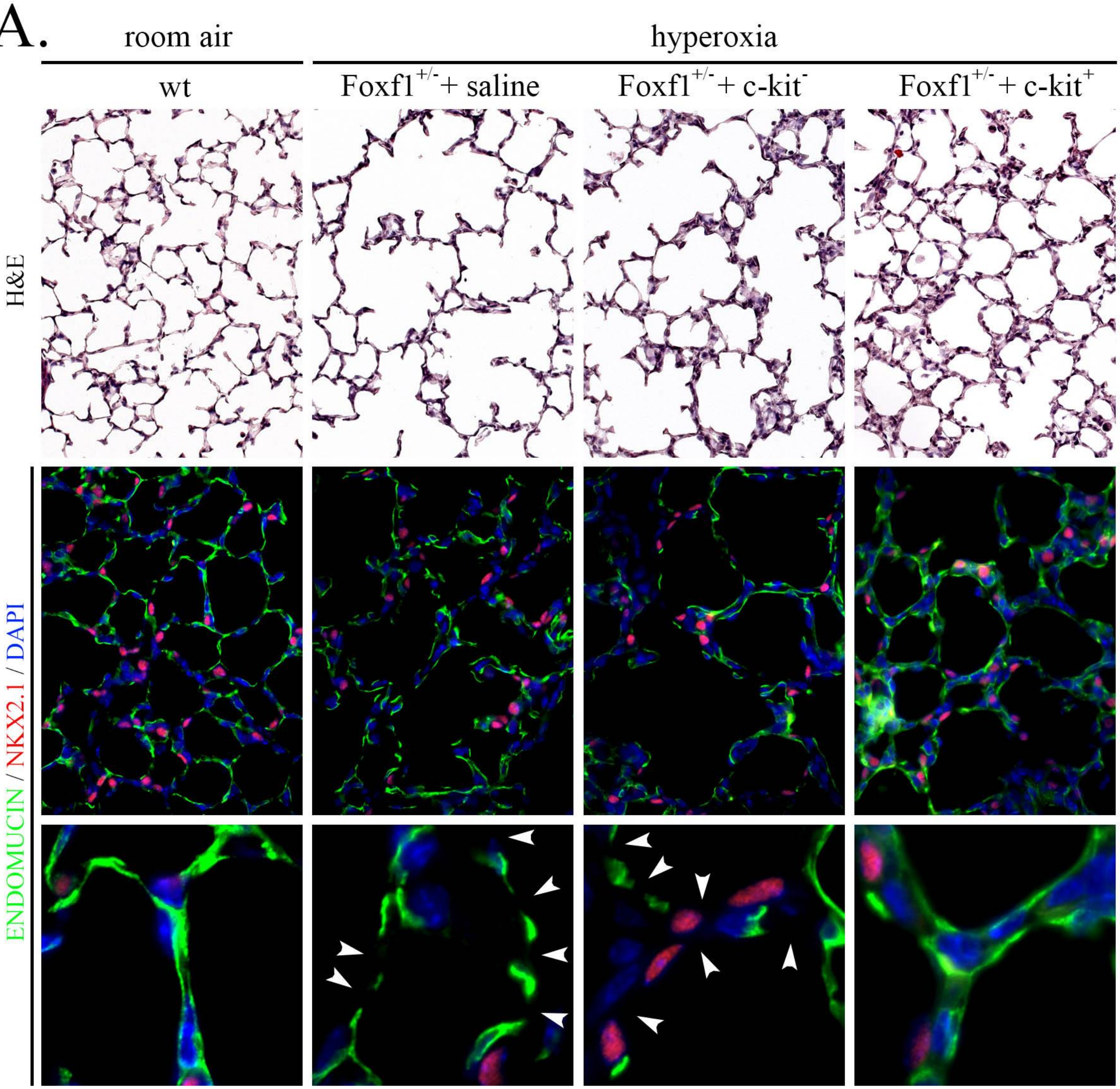
room air
hyperoxia
wt
Foxf1+/- + saline
Foxf1+/- + c-kit-
Foxf1+/- + c-kit+
H&E
ENDOMUCIN / NKX2.1 / DAPI

B.

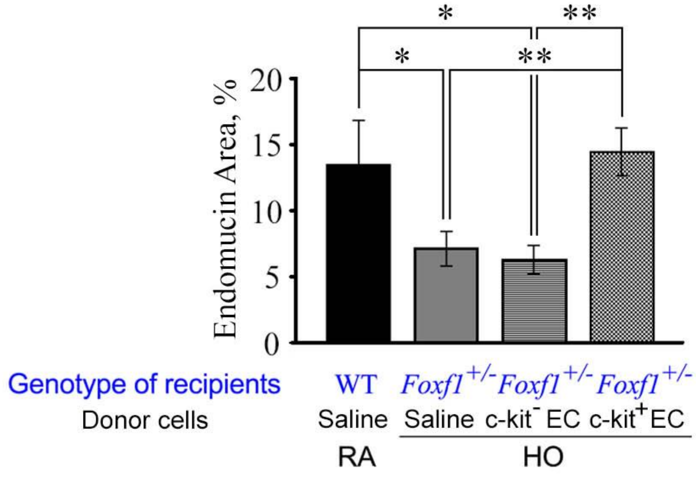
*
**
*
**
Endomucin Area, %
20
15
10
5
0
Genotype of recipients
Donor cells
WT
Saline
Foxf1+/-
Saline
Foxf1+/-
c-kit- EC
Foxf1+/-
c-kit+ EC
RA
HO

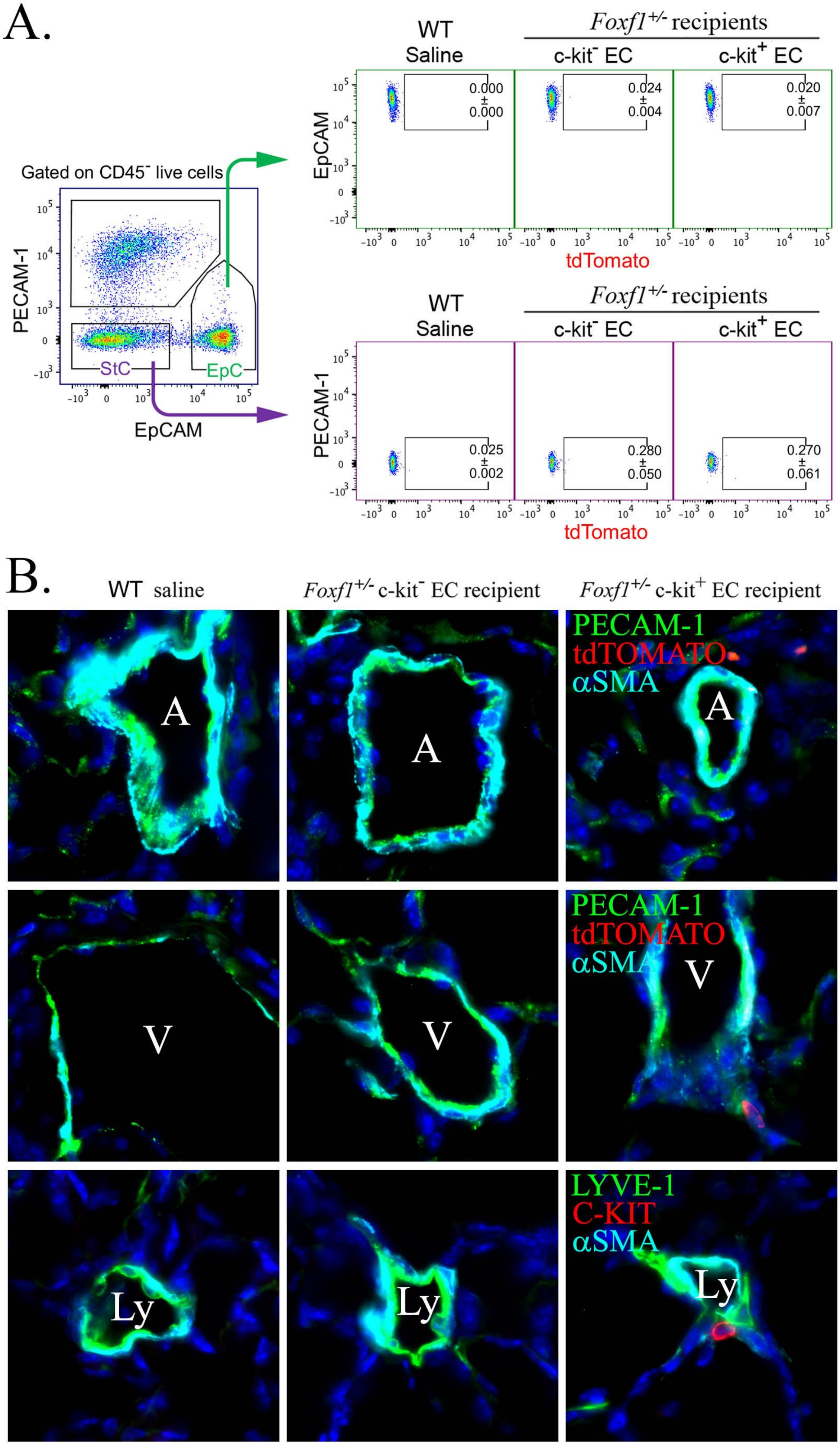
A.
Gated on CD45⁻ live cells
PECAM-1
EpCAM
StC
EpC
WT
Saline
Foxf1+/- recipients
c-kit⁻ EC
c-kit⁺ EC
EpCAM
tdTomato
0.000 ± 0.000
0.024 ± 0.004
0.020 ± 0.007
PECAM-1
tdTomato
0.025 ± 0.002
0.280 ± 0.050
0.270 ± 0.061
B.
WT saline
Foxf1+/- c-kit⁻ EC recipient
Foxf1+/- c-kit⁺ EC recipient
PECAM-1
tdTOMATO
αSMA
A
V
LYVE-1
C-KIT
αSMA
Ly

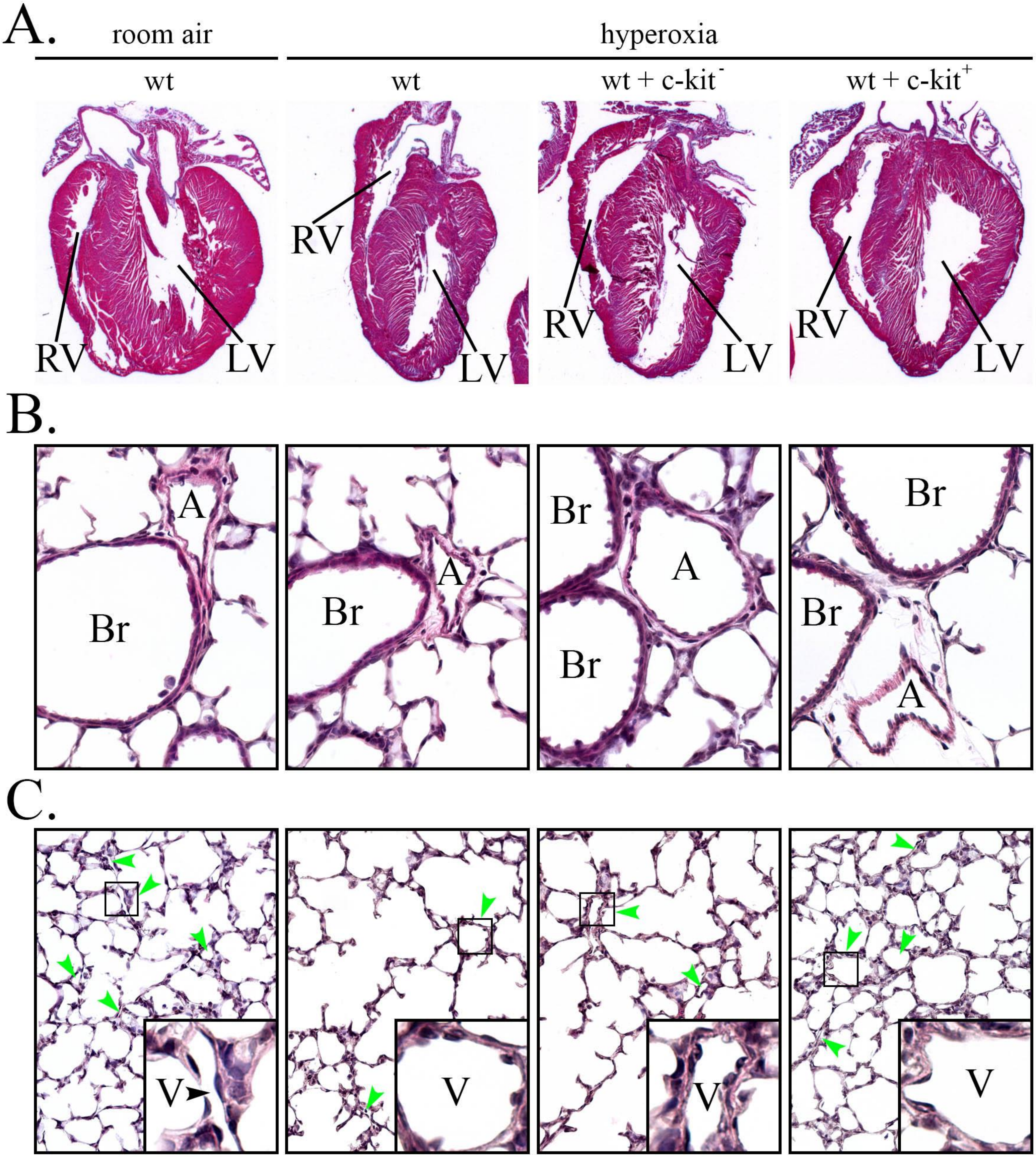
A.
room air
hyperoxia
wt
wt
wt + c-kit-
wt + c-kit+
RV
LV
RV
LV
RV
LV
RV
LV
B.
A
Br
A
Br
Br
A
Br
Br
Br
A
C.
V
V
V
V

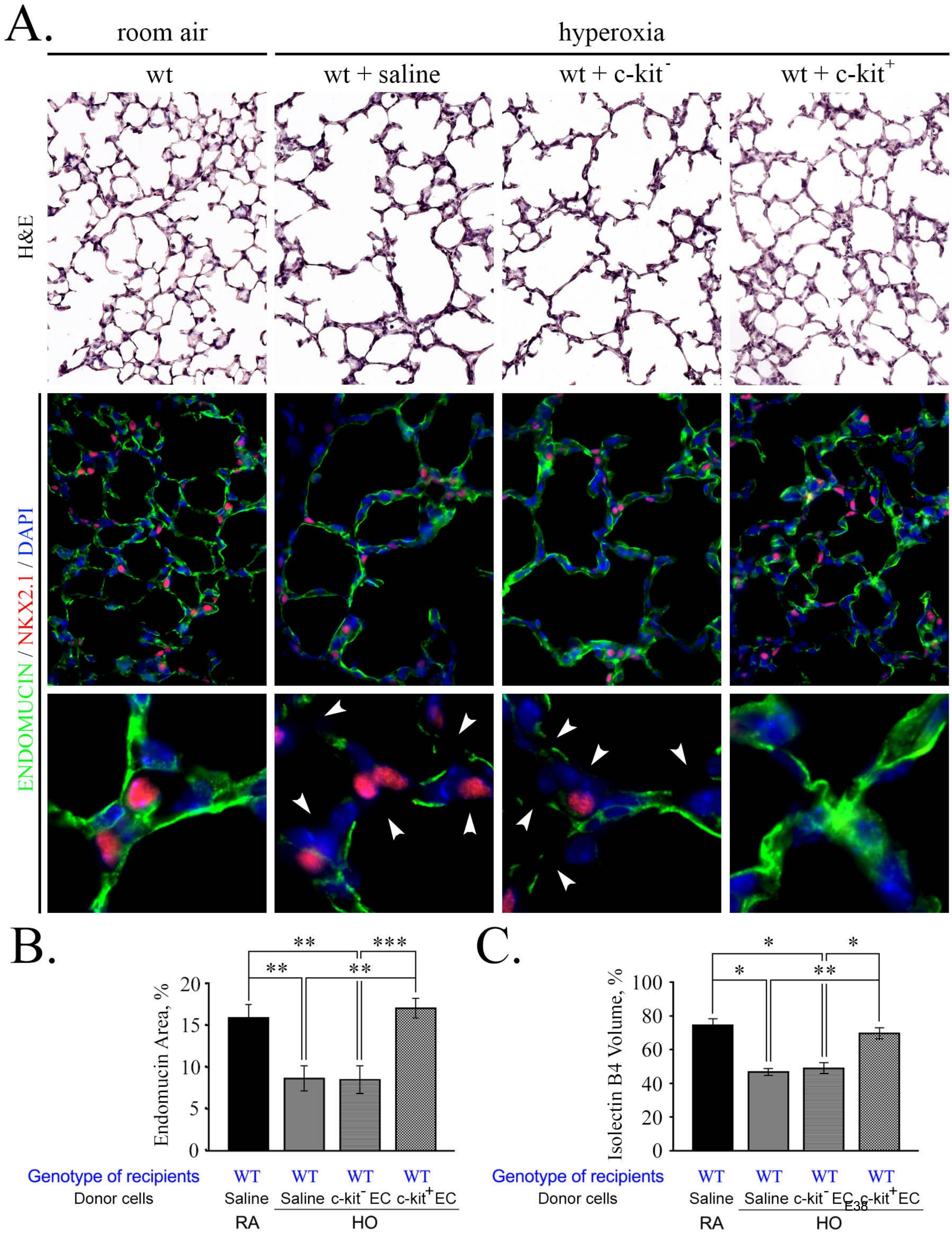
A.
room air
hyperoxia
wt
wt + saline
wt + c-kit-
wt + c-kit+
H&E
ENDOMUCIN / NKX2.1 / DAPI
B.
Endomucin Area, %
**
***
**
**
Genotype of recipients
Donor cells
WT
Saline
RA
WT
Saline
WT
c-kit- EC
WT
c-kit+ EC
HO
C.
Isolectin B4 Volume, %
*
*
*
**
Genotype of recipients
Donor cells
WT
Saline
RA
WT
Saline
WT
c-kit- EC
WT
c-kit+ EC
HO

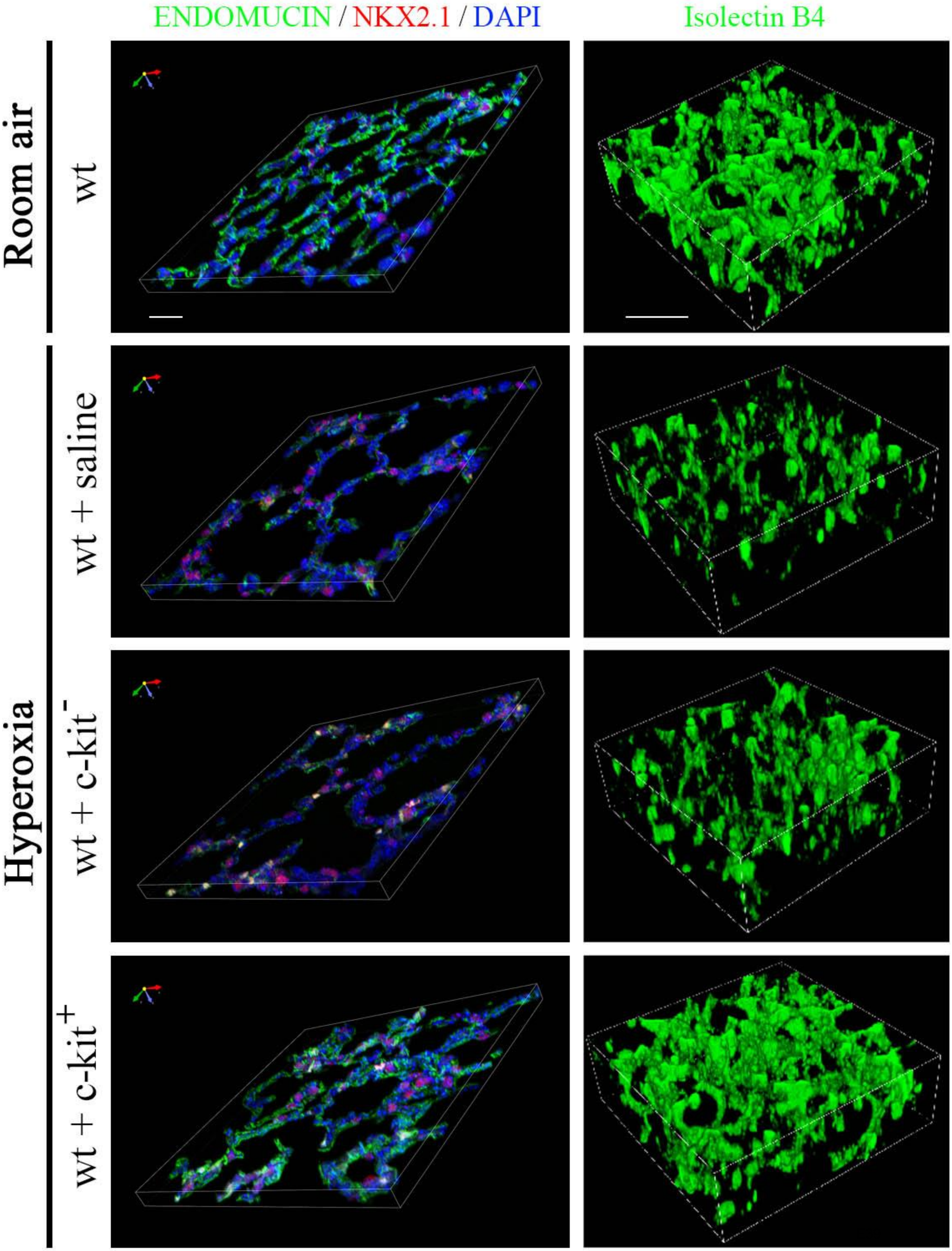
ENDOMUCIN / NKX2.1 / DAPI
Isolectin B4
Room air
wt
Hyperoxia
wt + saline
wt + c-kit⁻
wt + c-kit⁺

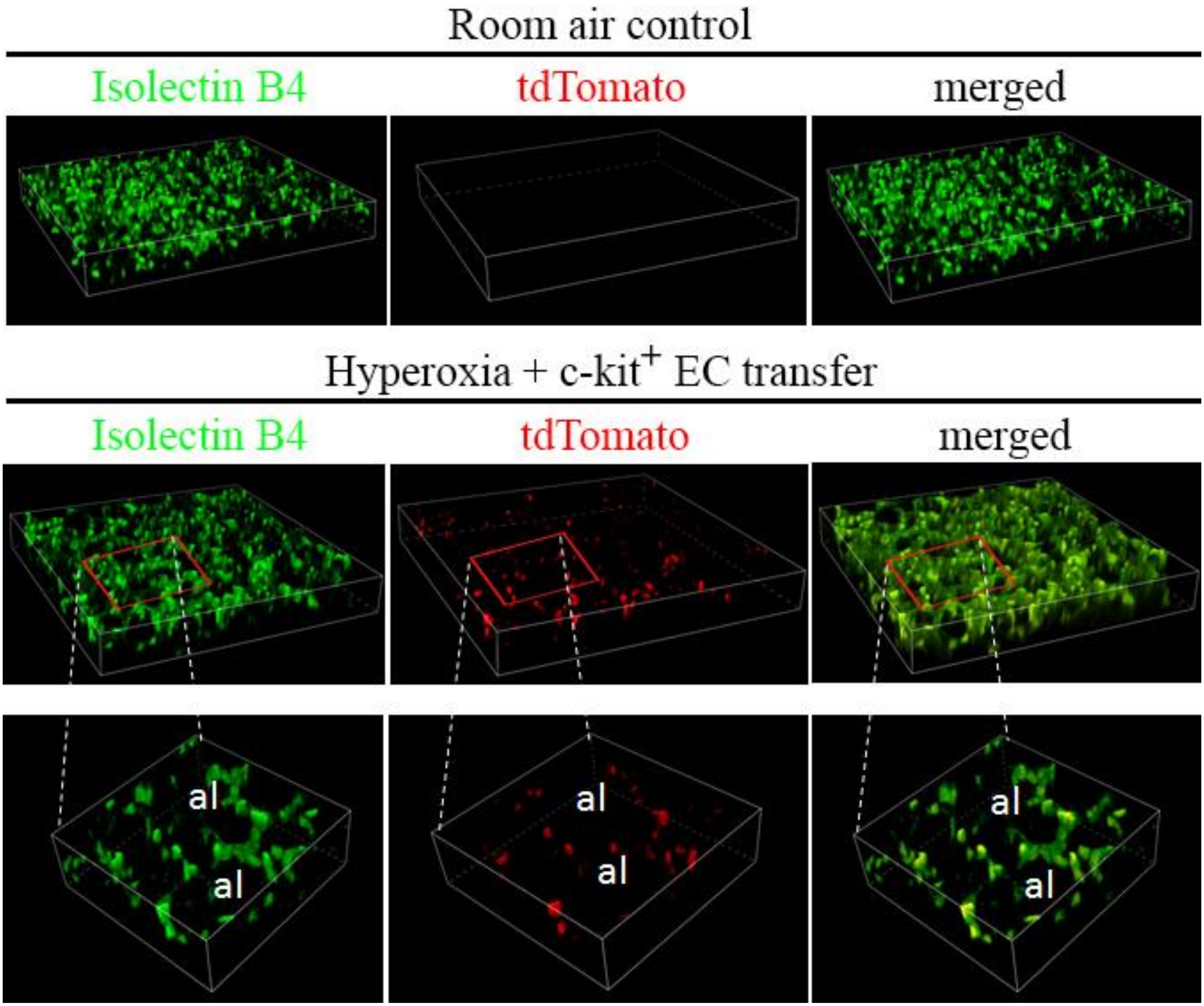
Room air control
Isolectin B4
tdTomato
merged
Hyperoxia + c-kit+ EC transfer
Isolectin B4
tdTomato
merged
al
al
al
al
al
al

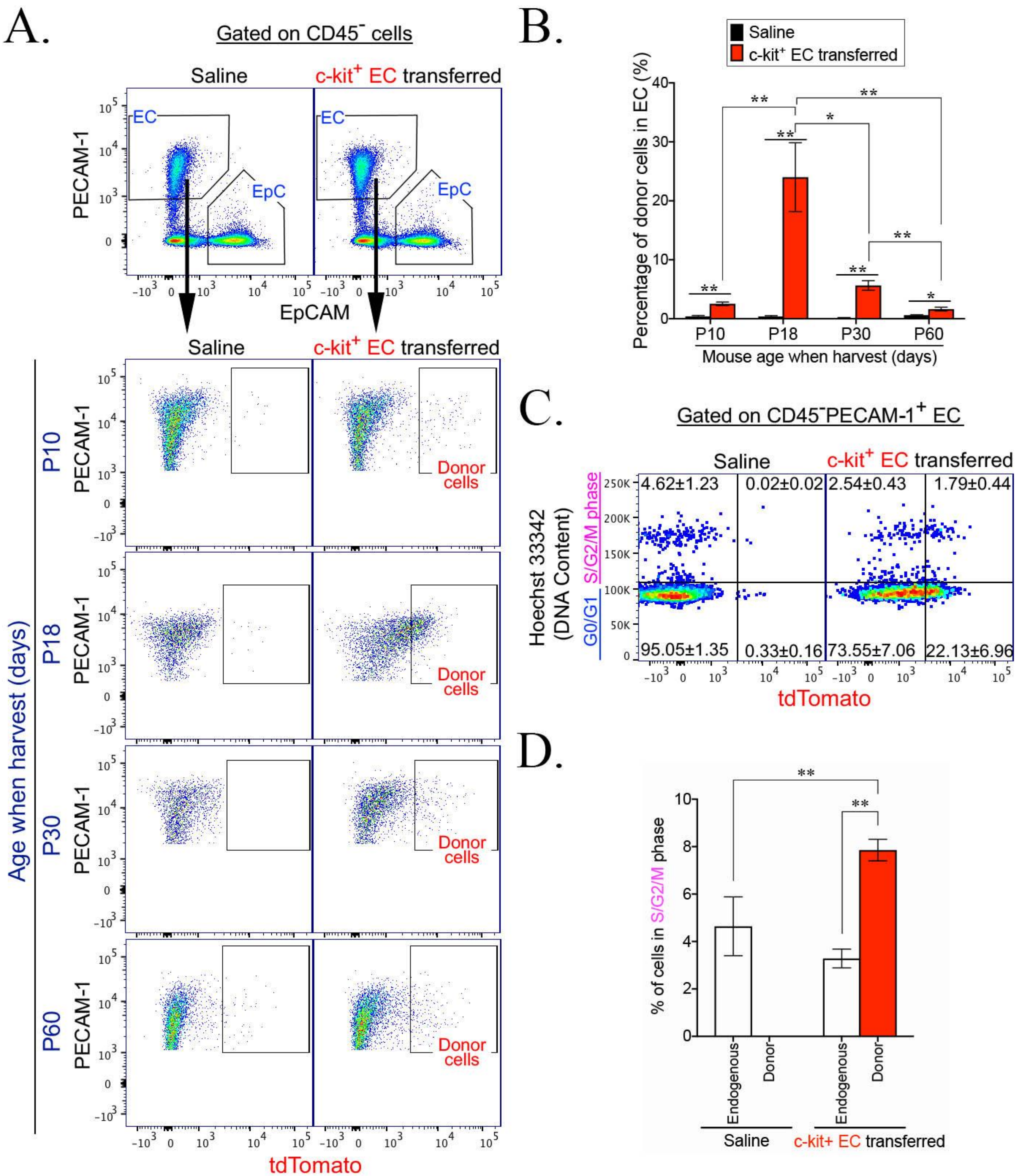
A.
Gated on CD45⁻ cells
Saline
c-kit+ EC transferred
EC
EpC
PECAM-1
EpCAM
Age when harvest (days)
P10
P18
P30
P60
Donor cells
tdTomato
B.
Saline
c-kit+ EC transferred
Percentage of donor cells in EC (%)
P10
P18
P30
P60
Mouse age when harvest (days)
C.
Gated on CD45⁻PECAM-1+ EC
Saline
c-kit+ EC transferred
Hoechst 33342 (DNA Content)
S/G2/M phase
G0/G1
4.62±1.23
0.02±0.02
2.54±0.43
1.79±0.44
95.05±1.35
0.33±0.16
73.55±7.06
22.13±6.96
tdTomato
D.
% of cells in S/G2/M phase
Endogenous
Donor
Endogenous
Donor
Saline
c-kit+ EC transferred